PYRIDINE-PEG FUNCTIONALIZED GRAPHENE NUCLEANTS FOR PROTEIN CRYSTALLIZATION

by

CEM MERİÇ

Submitted to the Graduate School of Engineering and Natural Sciences in partial fulfilment of the requirements for the degree of Master of Science

Sabancı University

Fall 2022

ABSTRACT

PYRIDINE-PEG FUNCTIONALIZED GRAPHENE NUCLEANTS FOR PROTEIN CRYSTALLIZATION

CEM MERİÇ

Materials Science and Nano Engineering, M.Sc. Thesis, December 2022

Thesis Supervisor: Assoc. Prof. Mustafa Kemal Bayazıt

Keywords: protein, crystallization, lysozyme, nucleant, graphene, pyridine, PEG

Structural characterization of proteins using X-Ray crystallography is crucial in protein-based applications. X-Ray crystallography requires protein crystals which can be grown using nucleants. Graphene and its derivatives are used as nucleants because they interact with proteins due to the hydrophobic and pi-pi stacking effect and increase protein concentration around their surface sites. Furthermore, polyethylene glycol(PEG) is another nucleating agent for protein crystallization. In this study, PEG-modified graphene nanostructures bearing positive charges are prepared as novel nucleants, and their nucleation ability is assessed. Pyridine-functionalized reduced graphene oxide (RGO-Pyr) is functionalized with three different PEG chains (PEG550, PEG2000, PEG5000), and octadecane (RGO-Pyr-OD). Six samples are tested as nucleants reduced graphene oxide (RGO), RGO-Pyr, RGO-Pyr-PEG550, RGO-Pyr-PEG2000 and RGO-Pyr-PEG5000. Protein crystallization is performed using the

hanging drop vapor diffusion method, and crystallization of lysozyme as model protein is monitored by a polarized light microscope. Protein crystals with good diffraction quality were obtained within 24 hours with all graphene nucleants except PEG2000, whereas control experiments with no graphene showed no crystals within the same period. The highest number of crystals was observed in droplets containing RGO due to the hydrophobic and pi-pi interactions between the RGO surface and lysozyme. RGO-Pyr produced a higher number of crystals with bigger sizes than PEGylated samples indicating a hydrogen bonding between the nitrogen atom of pyridine and lysozyme. The biggest crystals were obtained using RGO-Pyr-OD, attributed to the combined effect of pi and hydrophobic interactions arising from the positively charged pyridine and hydrophobic interactions between octadecane and lysozyme. The RGO-Pyr-OD shows promising potential as a novel nucleant for protein crystallization.

ÖZET

PİRİDİN-PEG İLE İŞLEVSELLEŞTİRİLMİŞ GRAFENİN PROTEİN KRİSTALİZASYONU İÇİN NÜKLEANT OLARAK KULLANIMI

CEM MERİÇ

Malzeme Bilimi ve Nano Mühendislik, Yüksesk Lisans Tezi, Aralık 2022

Tez Danışmanı: Doç. Dr. Mustafa Kemal Bayazıt

Anahtar Kelimeler: protein, kristalizasyon, lizozim, nükleant, grafen, piridin, PEG

Proteinlerin moleküler yapısının tayini için X-ışını kristallografisi en çok kullanılan yöntemdir. X-ışını kristallografisinde kullanılması için proteinlerin kristal yapıda olmaları gerekmektedir. Protein kristalleri çekirdeklendiriciler kullanılarak elde edilebilirler. Katmanlı yapıdaki grafen ve türevleri yüzeylerinde proteinler ile çekirdeklenmeyi temin edici etkileşimler kurulabilir. Bir başka çekirdeklendirici malzeme ise polietilen glikoldür (PEG). Bu çalışmada PEG ile işlevselleştirilmiş pozitif yük barındıran grafen malzemeler protein kristalizasyonu için geliştirilmiştir. Piridin ile fonksiyonalize edilmiş indirgeniş grafen oksit (RGO) yapısına 3 farklı molekül ağırlığına sahip PEG zincirleri (PEG550, PEG2000, PEG5000) ve oktadekan (RGO-Pyr OD) eklenerek protein kristalizasyonu üzerine etkisi incelenmiştir. RGO, RGO-Pyr, PEG550, PEG2000, PEG5000 ve RGO-Pyr-OD malzemeleri bu çalışmada çekirdeklendirici olarak denenmiştir. Protein kristalleri buhar difüzyon yöntemi ile lizozim proteini kullanarak elde edilmiştir. Lizozim kristalleri polarize ışık mikroskobu ile görüntülenmiştir. PEG2000

hariç denenen tüm nükelantlarda ilk 24 saat içerisinde kristal oluşumu gözlemlenmiştir. Nükleant kullanılmadan yapılan kontrol denemelerinde aynı zaman içerisinde protein oluşmamıştır. En fazla sayıda kristal, RGO kullanarak yapılan denemelerde elde edilmiştir. RGO'nun proteinler ile girdiği pipi ve hidrofobik etkileşimler bu gelişmenin sebebi olarak gösterilebilir. RGO-Pyr kullanılarak oluşturulan kristal sayısı da PEG kullanılarak oluşurulanlardan fazla olmuştur. Bunun sebebi, RGO-Pyr'in içerisindeki azot atomundaki elektron çiftinin lizozim ile hidrojen bağı kurmasıdır. Grafenin proteinler ile kurduğu pi-pi ve hidrofobik etkileşimler, piridin molekülündeki pozitif yük ve oktadekan ile lizozim arasındaki hidrofobik etkileşimler bir araya gelerek RGO-Pyr-OD malzemesinin en büyük kristalleri oluşturmasını sağlamışlardır. Bu sonuçlardan dolayı, bu çalışmada geliştilen RGO-Pyr-OD malzemesi protein kristallizasyonunda kullanım için potansiyele sahiptir.

ACKNOWLEDGEMENTS

I want to thank my supervisor, Assoc. Prof. Mustafa Kemal Bayazıt for his valuable support, tolerance, and guidance. I am grateful to have the opportunity to work in his research group NanoCHemCom. I also would like to thank every member of NanoCHemCom, and former members Cemre Irmak Kayalan and Pelin Duru, for contributing to my academic progress and being supportive working companions. I would like to thank Dr. Refik Arat and Tuçe Fidan to help me during my research. I also thank Dr. Mona Nejatpour for allowing me to explore different areas than my research subject.

I would like to thank my thesis jury members Assoc. Prof. Meral Yüce and Assoc. Prof. Hasan Kurt for their supervision and feedback to my thesis.

I would like to thank my undergraduate supervisor Prof. Dr. Gürbüz Güneş for his support during both my undergraduate and graduate studies. I value the time I spent in his laboratory at İstanbul Technical University.

I thank Assoc. Prof. Yuki Kaneko for allowing me to learn new methods of learning and teaching during my time as a teaching assistant for Nature of Science course.
I thank my friends Dr. Çiğdem Bilici, Mehmet Kahraman, Çağan Veziroğlu, Cahit Kulaç, Elisabeth Nagel, Evi Voetz, Kazi Sher Ahmed and Tuna Alp for their kindness and motivation.

I would like to thank my family for their moral support and guidance throughout my master's period. Special thanks to Can Akaoğlu for keeping a close eye on my progress.

TABLE OF CONTENT

LIST OF ABBREVATIONS

PEG : Poly(ethylene glycol)

GO : Graphene oxide

RGO : Reduced graphene oxide

RGO-Pyr : Pyridine-functionalized reduced graphene oxide

PEG550 : Pyridine-functionalized reduced graphene oxide further functionalized with PEG of 550-dalton molecular weight

PEG2000 : Pyridine-functionalized reduced graphene oxide further functionalized with PEG of 2000-dalton molecular weight

PEG5000 : Pyridine-functionalized reduced graphene oxide further functionalized with PEG of 5000-dalton molecular weight

RGO-Pyr-OD : Pyridine-functionalized reduced graphene oxide further functionalized with octadecane

DLS : Dynamic light scattering

TGA : Thermogravimetric analysis

UV-Vis : Ultraviolet-visible spectroscopy

M : Molar concentration

NaCl : Sodium chloride

µl : microliter

kDa : kilodalton

CHAPTER 1. INTRODUCTION

1.1. Thesis Overview

Structure determination of proteins and other molecules is essential for understanding biomolecules and has more practical outcomes such as drug development. Current methods for biomolecular structure determination include nuclear magnetic resonance spectroscopy and cryo-electron microscopy. These methods provide low-resolution data compared to the most used X-ray crystallography method. X-ray crystallography requires single protein crystals of 150 to 250-micron size. Producing single crystals with diffraction quality and enough size is challenging for proteins. Overcoming this challenge depends on additional materials called nucleants.

Protein crystallization takes place in two steps: nucleation and crystal growth. The nucleation step is where proteins form a nucleus due to attraction forces between them, such as hydrogen bonds, pi-pi interactions, electrostatic interactions or disulphide bonds, overcoming interfacial free energy. Crystal growth takes place after a critical nucleus size is reached. Due to the weak interactions between protein molecules, getting the critical size is problematic. Therefore, nucleants were developed with different mechanisms that attract the proteins. This attraction increases the local protein concentration and enables protein molecules to interact with each other and reach the critical size more quickly. Commonly used nucleation mechanisms include depletion due to osmotic pressure, physical trapping inside the pores, electrostatic attractions, hydrophobic interactions and hydrogen bonding. Recent strategies for protein crystallization are to have more than one mechanism in the same nucleant material.

It was shown before that graphene can attract protein molecules due to its hydrophobicity. The hydrophobic surface of graphene allows hydrophobic amino acids to be adsorbed to the surface. Furthermore, the carbon hexatomic structure of graphene forms pi-pi interactions with amino acids having aromatic residues, which also cause protein attraction. The attraction then increases the local protein concentration of proteins around graphene surface to higher levels than bulk concentration. The increased protein concentration around the graphene surface creates an environment more favourable to protein crystallization since crystal formation depends on saturation level.

In this thesis, functionalized graphene-based materials were synthesized, characterized, and tested as nucleants for lysozyme crystallization. Graphite was first functionalized with a pyridine molecule. With a lone pair on the nitrogen atom, pyridine can form hydrogen bonds with lysozyme. These electron pairs were utilized for attaching PEG with three different chain lengths (PEG550, PEG2000, PEG5000) and octadecane. Samples were characterized using Raman spectroscopy, X-ray photoelectron spectroscopy, thermogravimetric analysis, ultraviolet-visible spectroscopy, dynamic light scattering, Zetasizer and polarized light microscope. After the functionalization of these samples, pyridine becomes positively charged, allowing it to interact with negatively charged residues in lysozyme, which are aspartic acid and glutamic acid amino acids. Also, PEG and octadecane chains cause a depletion mechanism which is the osmotic pressure of these chains acting on proteins to increase their local concentration. These combined effects were compared in the ability to form crystals using the hanging drop crystallization method. Previous studies have shown that the additional functional groups can decrease the surface availability of graphene. Therefore, the additional PEG and octadecane may reduce the positive interactions between graphene surface and lysozyme, increasing the local protein concentration. The hanging drop experiments showed that RGO without any functionalized produces a higher number and size of crystals than PEGylated samples, which can be attributed to PEG's and octadecane's restriction of proteins to form pi-pi interactions and hydrophobic interactions with graphene surface. This result suggests that pi-pi interactions and hydrophobic interactions between lysozyme and graphene surface are more effective at attracting proteins than the effect provided by functional groups.

Furthermore, the positive charge of pyridine can be utilized to grow crystals with bigger sizes than the ones grown using porous nucleants. The lone pair electron of the nitrogen atom also performed better than PEG for inducing crystallization, suggesting a hydrogen bonding between pyridine and lysozyme. RGO-Pyr and RGO-Pyr-OD showed promising potential as novel nucleating agents for protein crystallization.

CHAPTER 2. PYRIDINE-PEG FUNCTIONALIZED GRAPHENE NUCLEANTS FOR PROTEIN CRSYTALLIZATION

2.1 Abstract

Structural characterization of proteins using X-Ray crystallography is crucial in protein-based applications. X-Ray crystallography requires protein crystals which can be grown using nucleants. Graphene and its derivatives are used as nucleants because their layered structure provides nucleation sites. Furthermore, polyethylene glycol(PEG) is another nucleating agent for protein crystallization. In this study, PEG-modified graphene nanostructures bearing positive charges are prepared as novel nucleants, and their nucleation ability is assessed. Pyridine-functionalized graphene oxide (RGO-Pyr) is functionalized with three different PEG chains (PEG550, PEG2000, PEG5000) and octadecane (RGO-Pyr-OD). Six samples were tested as nucleants reduced graphene oxide (RGO), RGO-Pyr, PEG550, PEG2000 and PEG5000. Protein crystallization is performed using the hanging drop vapor diffusion method, and crystallization of lysozyme as model protein is monitored by a polarized light microscope. Protein crystals with good diffraction quality are obtained within 24 hours with all graphene nucleants except PEG2000, whereas control experiments with no graphene showed no crystals within the same period. The highest number of crystals was observed in droplets containing RGO due to the hydrophobic and pi-pi interactions between the RGO surface and lysozyme. RGO-Pyr produced a higher number of crystals with bigger sizes than PEGylated samples

indicating a hydrogen bonding between the nitrogen atom of pyridine and lysozyme. The biggest crystals were obtained when RGO-Pyr-OD was used, attributed to the number of positively charged nucleation sites. RGO-Pyr-OD can be a promising and novel nucleant for protein crystallization.

2.2 Introduction

The high surface area of graphene and its exceptional thermal, mechanical and electrical properties make it one of the most studied materials. The properties of graphene can be further improved by attaching functional groups to its surface. In addition, hydrophobic interactions and pi-pi interactions can be formed between the graphene surface and proteins. Such qualities allow the use of graphene-based materials as nucleants for protein crystallization.

X-Ray Crystallography remains the primary method of determining the structure of biomolecules such as proteins. Despite the recent advances in imaging methods such as cryo-electron microscopy, 90% of the determined structures in Protein Databank are solved using X-Ray Crystallography. Obtaining crystals with good diffraction quality and size is still a challenge. Producing high-quality crystals is the rate-limiting step of solving structures of biomolecules which is essential for determining their function and new drug designs.

Proteins are made of covalently bonded amino acids. Carboxyl group and amino groups of different amino acids covalently bond to each other to form peptide bonds. The primary structure of proteins is the linear order of amino acids in their peptide chain. The spatial arrangement of amino acids, excluding their side chains, forms their secondary structure. In secondary structure, molecular interaction between proteins can result in helixes or sheets called α-helices and β-sheets, respectively. α-helices and β-sheets are connected by turns or by loops. The tertiary structure of proteins is the complete three-dimensional structure of the polypeptide chain, composed of all secondary structure elements and the side chains of each amino acid. In proteins with high molecular weight (>1000 kDa), if more than one polypeptide chain is present in the arrangement of different polypeptide chains is called the quaternary structure[1]. Protein crystals are held together due to attractive forces between various groups in the protein quaternary structure. In lysozyme crystals, the most dominant attractive force is hydrogen bonding.

Henn Egg White Lysozyme is one of the most characterized proteins and is often used as a model for protein crystallization, folding, unfolding and aggregation studies. The protein has a molecular weight of 14.3 kDa and comprises 129 amino acids from six α-helices and three β-sheets[2]. Lysozyme has a positive charge below its isoelectric point at pH 11. Six positively charged lysine amino acids and eleven positively charged arginine amino acids are present in the peptide chain, with negatively charged amino acids of seven aspartic acids and two glutamic acids, making the total charge positive[3]. The net positive charge of lysozyme molecules gives it advantages for adsorption on negatively charged surfaces. Furthermore, negatively charged amino acids are also available for electrostatic interaction with positively charged molecules.

A crystal is an ordered molecular structure composed of a repetition of a cell with a specific arrangement of molecules called the unit cell. Crystallization of molecules inside a solution is a first-order phase transition where crystal phases form out of supersaturated solution. Therefore, the crystallization of a molecule is driven by the supersaturation of the solution. The crystallization process is divided into two steps, namely nucleation and growth. The nucleation step takes place in the supersaturated phase of the solution. Due to particle agglomeration, a nucleus is formed in the nucleation step. After the nucleus reaches a critical size, the crystal growth step begins. Unlike the nucleation step, crystal growth occurs in the solution's metastable phase. In the crystal growth phase, a crystal is formed with the molecules joining the nucleus and crystal size is increased until the solution is depleted of the solute. The explanations of the nucleation step are based on classical nucleation theory, despite its shortcomings. In the following stages, the definition of classical nucleation theory, its shortcoming and new theories developed to solve the nucleation process will be discussed.

Classical nucleation theory is mainly based on the works of J.S. Gibbs and Volmer[4]. As mentioned earlier, crystallization is a first-order phase transition phenomenon characterized by concentration discontinuity on the phase boundary. Due to this discontinuity, a surface is formed. In the nucleation step, interfacial free energy at the surface must be overcome for molecules to form a cluster. The fluctuation can overcome this energy in concentration. In the first stages of nucleation, while the cluster size is small, changes in density can only cause a small number of particles to exceed the surface energy barrier and join the growing cluster. Only after the nucleus reaches a critical size the joining of other molecules to the cluster is energetically favourable. Assuming that the shape of the nucleus is spherical, this critical size of the nucleus is determined by the critical radius.

Nucleation happens in the small clusters of volume inside the large volume of the solvent. In order to transition into the crystal phase, the new phase's free energy should be lower than the old phase. This statement is only valid for the bulk part of the phase. Transition in the bulk phase always has negative free energy change and favours the phase transition. Whereas on the surface, the change of free energy differs. Since surface molecules are more loosely bound to each other than the molecules of bulk, the contribution of surface energy to free energy difference is higher than the bulk phase. Because the free energy of the surface is always positive, the higher free energy of the surface than the bulk can make the nucleation process unfavourable, especially at the beginning of nucleation when the size of the molecule is smaller. At the small nucleus size, most of the molecules of the nucleus lie at the surface, making the surface contribution to free energy dominant. At this stage, the nucleus is unstable, and the dissolution of nucleus is more favourable than its growth. The growth of the nucleus happens due to fluctuations in density. As the size of the nucleus increases, more molecules reside in bulk than surface making the total free energy positive. Because of this nucleus gets more stable as its size increases.

The positive sign of free energy at the surface comes from the contribution of the interfacial free energy, which can be defined as the free energy difference per molecule between the bulk of the nucleus and the surface of the nucleus. Interfacial free energy has a destabilizing effect on the nucleus. As the nucleus size increases, this effect is balanced by the negative contribution from the bulk free energy. At a critical size, the growth and dissolution of the nucleus have the same thermodynamic probably. This critical size is the critical radius of the nucleus. Critical radius is dependent on the interfacial free energy. High interfacial free energy means a bigger critical radius and decreases the probability of the growth of the cluster. A lower interfacial free energy favours the growth of the nucleus since it corresponds to a lower critical radius. A lower critical radius can also mean more possible nucleation sites inside the solution. This can cause smaller crystal size since the concentration of the protein inside the solution is limited and has to disperse into multiple nucleation sites. In such a case, crystallization can occur in a short time, in various places, and the solution can deplete the protein after a short time of crystal growth before more giant crystals are formed. Therefore, controlling the critical nucleus size, the possibility of crystallization, crystal size and the crystal number inside the solution can be variated.

The effect of nucleus size on free energy change during nucleation step can be quantified. For a spherical nucleus with a radius of r, the free energy change of process per molecule can be calculated using the equation:

$$\Delta g = \Delta g_b + \Delta g_s$$

$$\Delta g = -(\frac{4/_3 \pi r^3}{\Omega} \Delta u) + 4\pi r^2 \alpha$$

Where Δg is the free energy change per molecule, Δg_b is the contribution from the bulk of the solution and Δg_s is the surface contribution. Ω and α are volume per molecule and interfacial free energy, respectively. The free energy contribution from the bulk solution is always negative and dependent on r^3, whereas the free energy contribution of the surface phase is always positive and dependent on r^2. We can therefore see that as r increases, the free energy from bulk increases more than the free energy of the surface. Since the first term is negative and the second term is positive higher r values make the total free energy negative and the nucleation process favourable.

The critical radius value can be found by setting the derivative of the sum of free energy from bulk and free energy of the surface to zero.

$$\frac{d\Delta g}{dr} = 0$$

$$r_c = 2\Omega\alpha/\Delta u$$

$$r_c = 2\Omega\alpha/kT\sigma$$

The sum of free energies is maximum when the radius has the r_c value. This means that free energy change for increasing and decreasing the radius size is negative. Therefore, both processes are thermodynamically favourable when the nucleus has a critical radius.

By decreasing the interfacial free energy, it is possible to improve the crystallization process. Since interfacial free energy is a barrier that must be overcome to create a stable nucleus, finding new substrates with less interfacial free energy between proteins in the solution and themselves than proteins in the solution and growing crystal. Foreign surfaces, therefore, can be introduced to form stronger bonds with the protein molecules than solvent. This would result in decreased interfacial free energy, and the foreign surface acts as a site which attracts proteins. Due to increased protein concentration at the surface, nucleation and crystal growth steps take place at the surface more easily. This method is called heterogeneous protein crystallization and can be quantified by modifying the homogenous crystallization equations given above.

In homogenous crystallization, there is only one interfacial energy between the solution and the protein crystal. To modify the equation, new interfacial energies are introduced. Two new interfacial energies are introduced between the crystal and the foreign surface, denoted as α_{cf}, and the other between the liquid and the foreign surface denoted as α_{lf}.

The interfacial free energy between the protein crystal and the liquid, used in homogenous nucleation, is denoted as α_{cl}. The expression for heterogenous nucleation therefore becomes:

$$\Delta g = -(\frac{4/_3 \pi r^3}{\Omega} \Delta u) + \pi r^2 (2\alpha_{cl} + \alpha_{cf} - \alpha_{lf})$$

The critical radius for heterogeneous crystallization can then be expressed as:

$$r_c = 2\Omega\alpha'/kT\sigma$$

$$\alpha' = \alpha_{cl}(1 - \frac{\alpha_{lf} - \alpha_{cf}}{2\alpha_{cl}})$$

A foreign surface can reduce the total interfacial free energy when the interfacial free energy between the crystal and foreign surface is less than the interfacial free energy between the liquid and the foreign surface. In this case, the term inside the brackets is less than one made α_{cl} greater than α'. Reduced interfacial free energy results in a lesser size of the critical radius, meaning that introducing foreign surfaces that can make stronger bonds with crystals than the solvent and do not make more robust bonds with the liquid than the crystal improves the crystallization probability by reducing the critical nucleus size required for protein crystallization.

The foreign surfaces utilized for protein crystallization can be porous surfaces. Porous surfaces mechanically trap protein inside their pores. Trapped proteins then interact with each to form crystals. The first attempt using porous substrates for growing crystals was made using mesoporous silicon[5]. The material had various pores, with average pore size between 5 nm and 10 nm and was used for crystallizing lysozyme, catalase, thaumatin, concanavalin A, phycobiliprotein and trypsin. Stokes' radii of all the proteins mentioned were between 2 nm and 5 nm. The crystal growth was observed on the silicon surface for all the proteins tested except concanavalin A. The crystallization occurred in metastable conditions, which is nonspontaneous for nucleation, and large crystals with good diffraction quality were obtained. The study concluded that the size distribution of the silicon pores allows proteins of different sizes to attach to the surface. The major drawback of using mesoporous silicon is its stability. Mesoporous silicon is only usable for several weeks before oxidation of the material result in blockage of its pores[8]. Another study used commercial porous glass with pore sizes varying between 10 nm and 100 nm to produce crystals of lysozyme, apoferritin and thaumatin[6]. Saturation conditions were chosen lower than the saturation required for crystallization on the standard poreless glass. As a result, larger and more crystals were obtained on the porous glass surface, whereas almost no crystals were developed on the traditional glass surface. Better qualities of the crystals obtained from the porous surface are due to the lower saturations required since crystals grown at lower saturation conditions show better qualities[7]. Bio glass is another porous medium studied as a nucleant surface. It was demonstrated that a mesoporous gel-glass surface with the formula of $CaO–P_2O_5–SiO$ and pore sizes varying between 2 nm-10 nm produced crystals of seven different proteins at metastable saturation[9].

Poly(ethylene glycol)(PEG) is one of the most used crystallizing agents in protein crystallization studies[10]. PEG molecules induce a molecular attraction between protein molecules which can result in nucleation and crystal growth. This attraction is due to the depletion force due to PEG acting on the protein molecules. When two protein molecules get closer, the PEG chain is excluded between the two protein molecules. Since PEG has high osmotic pressure, the exclusion of PEG between protein molecules creates a depletion force, pushing proteins to each other[11].

Another strategy to produce protein crystals is to use a charged surface. Proteins are charged molecules and are able to form electrostatic interactions with oppositely charged surfaces or functional groups. These electrostatic interactions are strong enough to reduce the interfacial free energy barrier and increase the local supersaturation required for protein nucleation[12]. A study utilized mica surface with ionizable groups of 3-aminopropyltriethoxysilane for concanavalin A, lysozyme and thaumatin crystallization. The study found that ionizable groups at the mica surface reduce crystallization time and the saturation required for concanavalin A and thaumatin. The crystallization effect was attributed to electrostatic interactions between ionizable groups on the mica surface and protein molecules[13]. Another study demonstrated the effect of charged groups using sulfonated polystyrene films and amino-silanized mica sheets as surfaces for nucleation[14]. The electrostatic interactions between protein crystals and the ionizable groups on the surface of mica sheets and polystyrene films had a stabilizing effect on protein crystals. Charged surfaces can also be utilized to control the growth of crystals in specified directions. By creating a charge on the nucleation surface opposite of the protein, the direction of crystal growth of lysozyme was successfully controlled[15].

Graphene is a highly studied material that can attract proteins to adsorb into its surface. The aromatic residue of amino acids and hexatomic carbon rings of graphene attract each other due to pi-pi interactions. Moreover, graphene is a hydrophobic surface, and proteins contain hydrophobic amino acids. In order to minimize its surface to the water, in the presence of graphene, proteins interact with the graphene surface via hydrophobic interactions. These two interactions of graphene and proteins cause protein adsorption onto the graphene surface[16]. This phenomenon, in turn, increases the local protein concentration around graphene. Due to the increased concentration, protein crystallization is more favorable around the graphene surface than bulk protein solution. In addition, defects in the carbon structure of the graphene layer can trap protein molecules and increase the protein concentration needed for crystallization. The adsorption of protein changes its tertiary structure. A model has shown that lysozyme adsorbs onto the graphene surface with aromatic and hydrophobic residues coming into contact with the surface[16]. Another study has shown that after desorption, proteins take a different folding than their natural shape. Still, the enzymatic activity of lysozyme is unhindered, meaning that active sites lysozyme are not damaged due to the interactions with graphene[17]. Due to the slow residence time of lysozyme on foreign surfaces, the denaturation of proteins due to intramolecular attractions is often neglected[8].

The approaches mentioned above can be combined to develop nucleants for protein crystallization. The effect of surface charge, hydrophobicity, pi-pi interactions and depletion mechanism on protein crystallization can be used in single nucleant. Such materials can be carbon nanomaterials since they can form attractive interactions between their surface and protein molecules. Furthermore, they can be functionalized with groups of surface charge and groups that produce a depletion effect. A study showed that the number of drops containing protein crystals in the hanging drop method was improved using colloidal graphene and graphene oxide as nucleants[18]. Another carbon nanomaterial tested was carbon nanotubes. The porosity of carbon nanotubes allowed nucleation and crystal growth on lower saturation levels[19]. A comparative study was made using carbon nanotubes, graphene oxide and carbon black functionalized with different groups such as amines, thioether and hydroxyl, with the emphasis being on polyethylene glycol with 5 kDa molecular weight[20]. Out of the 20 carbon nanomaterials tested polyethylene glycol-functionalized carbon black nanoparticles were the most effective material due to the depletion effect of PEG, surface interactions between carbon black and proteins, surface area and surface topography of carbon black. Another study compared PEG-functionalized multi-walled carbon nanotubes, single-walled carbon nanotubes, exfoliated few-layer graphite, graphite nanoplatelets and carbon black as nucleants for protein crystallization[21]. The study concluded that carbon nanotubes effectively induce nucleation and crystal growth. Still, the PEG functionalized exfoliated few-layer graphite and graphite nanoplatelets were more successful than carbon nanotubes at single crystal production. A further study showed that a lower ratio of PEG attachment on the graphene surface proved more effective for crystallization[22].

In this thesis, we have developed novel nucleants for protein crystallization by functionalizing reduced graphene oxide(RGO). RGO was first functionalized with pyridine. The lone pair of pyridinic nitrogen was further utilized for grafting polyethylene glycol with three different chain lengths: 550 Da, 2000 Da and 5000 Da. Also, one sample was functionalized with an octadecane chain instead of PEG. We have tested six materials to compare their nucleating properties, namely: reduced graphene oxide(RGO), pyridine functionalized reduced graphene oxide(RGO-Pyr), three different PEG grafted RGO-Pyr materials (PEG550, PEG2000, PEG5000) and octadecane grafted RGO-Pyr (RGO-Pyr-OD). The positive effect of reduced graphene surface on protein crystallization was increased using the electron pairs of pyridine molecule, the positive charge of pyridine in chain grafted samples and the depletion effect of polyethylene glycol. Crystallization studies were conducted using the hanging drop vapor diffusion method and lysozyme as a model protein.

2.3 Experimental

PEG with molecular weights of 550 Da, 2000 Da and 5000 Da were purchased from Sigma Aldrich. Graphite was purchased from Alfa Aesar Company.

For the synthesis of pyridine functionalized reduced graphene oxide, a solution of $NaNO_2$ (7,10 mmol) at 0 °C was dissolved in 0,7 ml of water at the same temperature. The solution was then added dropwise to 5 mL of 4 M HCL solution at 0 °C containing 6,99 mmol of 4-amino-pyridine. After stirring for 30 minutes while maintaining the 0 °C temperature, a yellow solution was obtained. Next, 10 mg reduced graphene oxide was dispersed in 20 mL of *N, N*-dimethylformamide at 0 °C via ultrasonic bath for 5 minutes and then added dropwise to the previously prepared solution. The resulting mixture was stirred at 0 °C for 4 hours. After 4 hours, the mixture was allowed to reach room temperature while stirring for 15 hours. The mixture was then filtered through a 0,2 µm nylon membrane (Whatman) to obtain functionalized reduced graphene oxide. The functionalized sample was then dispersed in 100 mL, 2M HCl, before filtering and washing until pH was neutral. To provide deprotonation of pyridinium salt to pyridine, the solid sample was redispersed in 100 mL 2 M NaOH and stirred overnight. Functionalized reduced graphene oxide was then filtered using 0,2 µm membrane and washed with water until neutral pH was reached. Dispersion and filtration processes were repeated separately using first 2x30 mL THF, then 2x30 mL acetone and finally 2x30 mL acetone as solvents. Pyridine functionalized reduced graphene oxide was obtained after drying at 80 °C overnight.

To attach methoxy-terminated PEG (mPEG) into RGO-Pyr, mPEG was first converted to chloro-terminated PEG (mPEG-Cl) by reaction with thionyl chloride following a literature procedure[23]. mPEG-Cls of 550 da, 2000 da and 5000 da (45,09 mmol) and 1-bromooctadecane were separately added to a dispersion of RGO-Pyr (5 mg) in dry DMF (10 mL), dispersed using an ultrasonic bath (ISOLAB 621.05.006, 180 Watt) for 5 minutes, and the reaction mixture stirred at 60 °C overnight. The RGO-Pyr-mPEGs were then filtered through a PTFE membrane (0,2 µm, Whatman), redispersed in acetone (30 mL), filtered and washed with acetone (2x 30 mL) and dried overnight at 80 °C to afford PEGylated RGO-Pyr and octadecyl modified RGO-Pyr similar to a previous study reported on literature[24].

Raman spectra were taken from the powder samples on a silicon wafer using Renishaw Raman spectroscopy having a laser beam of 532 nm wavelength. Analysis was performed under 10% laser power, 20 exposure and two accumulations settings.

Sample dispersions were prepared initially at 30 µg/mL sample concentration on water. Dispersions were then sonicated for 2 hours. After sonication, dispersions were left to settle for 30 minutes. The middle part of the solution in the vial was assumed stable after 30 minutes and taken via pipette, leaving only supernatant and sediment fractions inside the vial.

The concentrations of the stable parts of the samples were determined using UV-Vis spectroscopy and Lambert-Beer's law. 2 minutes of sonication was performed before each UV-Vis spectroscopy analysis. Then, the dispersions are further diluted to around 3,50 µg/mL to obtain the same concentration of samples for further analysis.

Zeta potential analysis was done on dispersed samples using Malvern Zetasizer. Before each analysis 2 minutes of sonication was performed on every sample.

The hanging drop crystallization method was performed in 24 well plates. Buffer solution 4.7 pH and 1M NaCl concentration were prepared to be used in droplets. Another buffer solution with a 4.7 pH and 3M NaCl concentration was prepared to be used in 24 well plate reservoirs. An increased NaCl concentration facilitates vapor diffusion between the reservoir and the droplet. Inside the buffer solution, lysozyme was added at 66 mg/mL concentration, and the solution was mixed gently without stirring. 1.5 µL of buffer solution was mixed with 0.5 microliters of sample dispersion to obtain 2 µL droplet volume. The total composition of the droplets is 50 mg/mL lysozyme, 75 µg/mL sample dispersions and 1 M NaCl for droplets containing nucleants. The control sample having no nucleant, only contains 50 mg/mL lysozyme and 1 M NaCl. Droplets were prepared on a glass surface with greased corned, which were then sealed on top of the 24 well plates containing 800 µL of 4.7 pH and 3M NaCl reservoir condition. Images of the droplets were taken after preparation and every 24 hours using Nikon SMZ1500 polarized light microscope.

2.4 Results and Discussion

Raman spectroscopy is an analysis method that gives information about the vibrational mode of a material by subjecting it to a beam of irradiated light and measuring the amplitude of inelastic (Raman) scattering[25]. The sample is subjected to light of a specific wavelength that is either absorbed or scattered when interacting with the sample. Light can be scattered in two ways: elastic or inelastic. Most photons are scattered elastically, resulting in no wavelength change. However, wavelength change happens in an inelastic scattering of photons. This change due to inelastic scattering is called the Raman shift. In elastic scattering, the wavelength change creates an energy exchange related to the change in the vibrational or rotational energy of the sample. The change in the rotational or vibrational energy of the sample is, in turn, related to specific chemical bonds[26].

Raman spectra of carbon nanomaterials show three distinct bands, namely D, G and 2D bands. The D band is around 1350 cm^{-1} and is a measure of defects in the graphene layers, such as vacancies or dislocations[27]. The location of the G band is near 1580 cm^{-1} and is due to in-plane vibrations caused by sp^2 hybridized carbons. The number of graphene layers is the cause of the appearance and the shift of the 2D band near 2700 cm^{-1}.

The ratio of the D band to the G band (I_D/I_G) is generally used as a measure of defect densities on graphene layers[28]. For graphite with a highly ordered structure, the relatively weak D band is mainly caused by disorders present at the edges, whereas the G band is visible due to the in-phase vibration of the graphitic lattice[29]. Because there are no strong D bands for graphite, the I_D/I_G value is insignificant. Oxidation of graphite introduces disorders to the lattice, causing an increase in the D band and broadening of the D and G bands. Reduction of graphene oxide further increases the intensity of the D band since sp^2 carbons are restored during the removal of oxygen groups during the reduction process[30]. Therefore I_D/I_G value increases after the reduction of graphene oxide to reduced graphene oxide.

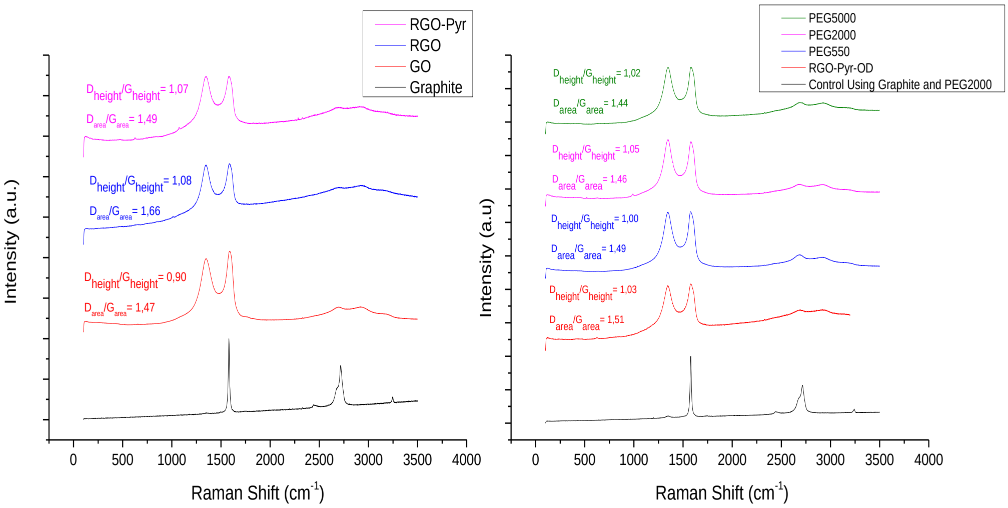

Figure 1. Raman spectra of base graphite, graphene oxide, reduced graphene oxide and functionalized graphene samples

In our Raman spectra experiments, we have two control samples: graphite and a physical mix of graphite and PEG 2000 (control using graphite and PEG 2000). As expected, the graphite sample showed a strong peak around the G band. Still, it did not show a D band with high intensity (Fig. 1). Similarly, D band intensity for control using graphite and PEG2000 is insignificantly low, suggesting that no chemical interactions were formed between PEG2000 and graphite during the physical mixing. After the oxidation of graphite to graphene oxide intensity of the D band is increased. During the reduction process, removing oxygen and increasing the sp^2 hybridization of carbons caused a further increase in the D band. An increase of I_D/I_G value from 0,90 to 1,08 was observed between GO and RGO. The results suggest successful oxidation and reduction of graphite to GO and RGO. The attachment of pyridine to the RGO surface and further attachments of polyethylene glycol and octadecane caused no significant changes in the Raman spectra.

Scanning electron microscope images of the RGO-Pyr sample were taken to evaluate the material's porosity. Proteins can accumulate in pores with radii lower than 1 µm but this pore length is not enough to affect protein crystallization. On the other hand, proteins trapped in pores having a much smaller pore length of around 5-10 nm can reach a critical saturation level to produce crystals. The smallest pore length in our scanning electron microscope images was

20 nm. Therefore, it can be said that the crystallization effect of our functionalized graphene samples is not due to the material's porosity.

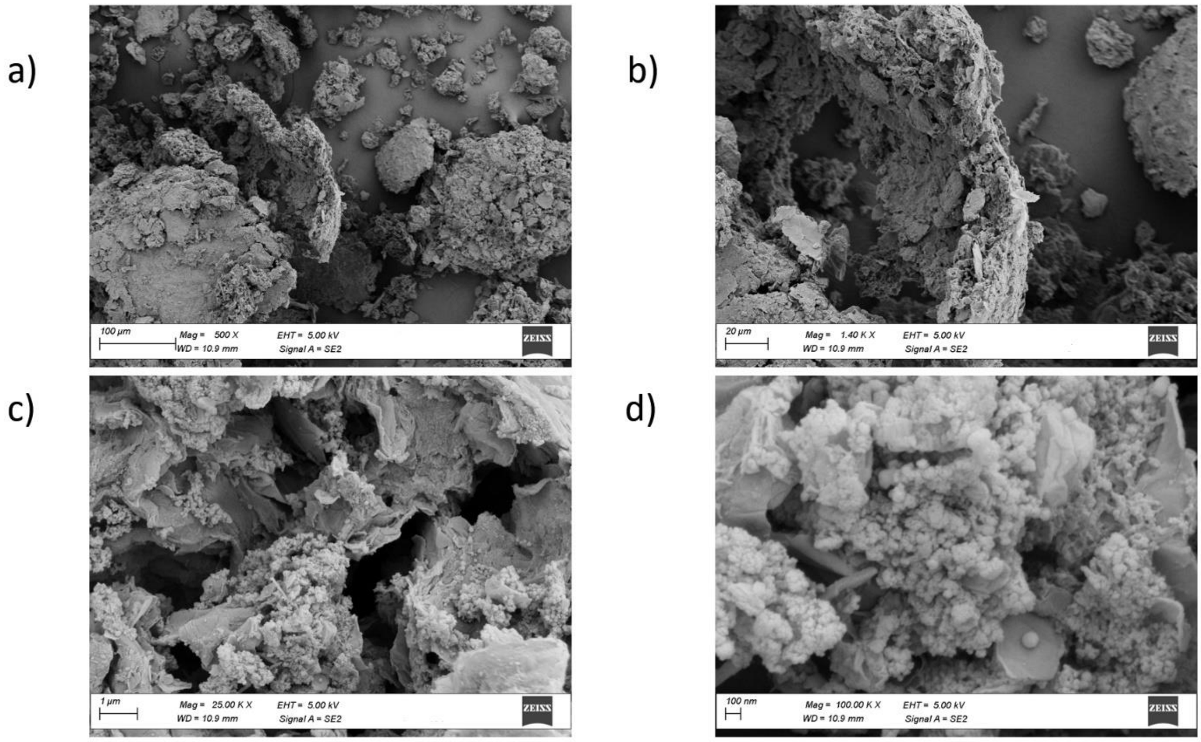

Figure 2. Scanning electron microscopy of RGO-Pyr at a) 500 x, b) 14000 x, c) 25000 x and d) 100000 x magnitudes

Dynamic light scattering (DLS), also called quasi-light scattering or photon correlation spectroscopy, is an analysis method for determining the size of particles in a colloidal suspension. When dispersion is subjected to monochromatic light, the Brownian motion of the particles inside the solution causes the light to scatter. Since the particles' Brownian motion depends on the particle size, smaller particles diffuse faster. In contrast, bigger particles diffuse slower, and particle size can be determined by measuring the scattering of light[31]. Dynamic light scattering uses a light source and a detector to detect to scattered light caused by particles in a solution. The detection signal is evaluated over time to obtain the diffusion coefficient. The diffusion coefficient can then be used to calculate average particle size (hydrodynamic radius) by using the Stokes-Einstein equation:

$$D = k_b T / 6\pi\eta R_H$$

Where k_b is the Boltzmann constant, T is absolute temperature, η is solution viscosity, R_H is the hydrodynamic radius, and D is the diffusion coefficient[32]. DLS equipment contains a program to calculate hydrodynamic radius using measured diffusion coefficient and Stokes-Einstein equation.

Graphite particles consist of layers held together by pi-pi interactions, which can be separated by additional forces introduced between the layers[33]. Attaching functional groups to graphite can present forces to push the graphene layers apart[34]. Electrons of the functional groups can create electrostatic repulsion between graphene layers, reducing the particle size.

Table 1. Average particle size and zeta potential of reduced graphene oxide and functionalized samples

Sample	Average Particle Size (nm)	Zeta Potential (mv)
RGO	1287 ± 312	-21.9 ± 2.6
RGO-Pyr	229 ± 23	-28.6 ± 2.0
PEG550	897 ± 51	-11.3 ± 1.5
PEG2000	840 ± 181	-16.2 ± 3.2
PEG5000	1170 ± 187	-38.1 ± 2.0
RGO-Pyr-OD	842 ± 149	-17.2 ± 1.6

The average particle size of RGO samples was 1287.68 ± 312.85 nm (Table 1). The average particle size was reduced to 229.22 ± 23.51 nm after pyridine attachment to RGO. The resulting decrease can be due to the coulombic repulsion caused by electrons introduced by pyridine between the graphene layers RGO overcoming the pi-pi attractive forces holding graphene layers together. After PEGylation and octadecane addition, the average particle size was increased due to long PEG and octadecane chains attached to RGO-Pyr. PEG and octadecane chains can increase the average particle size by connecting more molecules to the RGO and decreasing the effect due to additional coulombic repulsion force from PEG and octadecane molecules pushing graphene layers apart. This double effect can be why PEG550 has a larger average particle size than PEG2000 despite the longer chain of PEG2000 compared to the chain of PEG550. PEG 5000, having the highest molecular weight and long chain, showed larger particle sizes than the other PEGylated and octadecane functionalized samples.

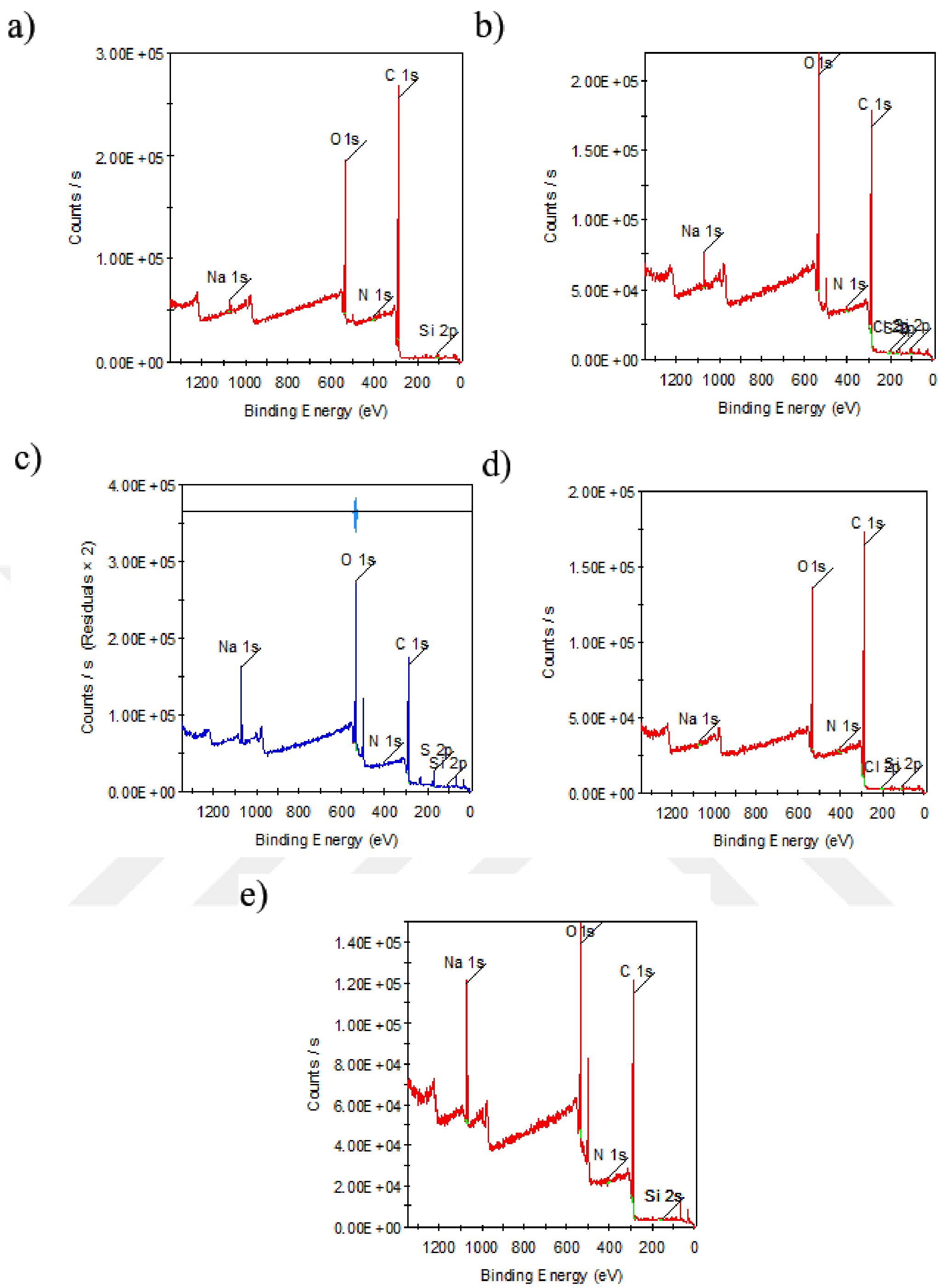

Figure 3. X-ray photoelectron spectroscopy surveys of a) RGO-Pyr, b) PEG550, c) PEG2000, d) PEG5000, and e) RGO-Pyr-OD

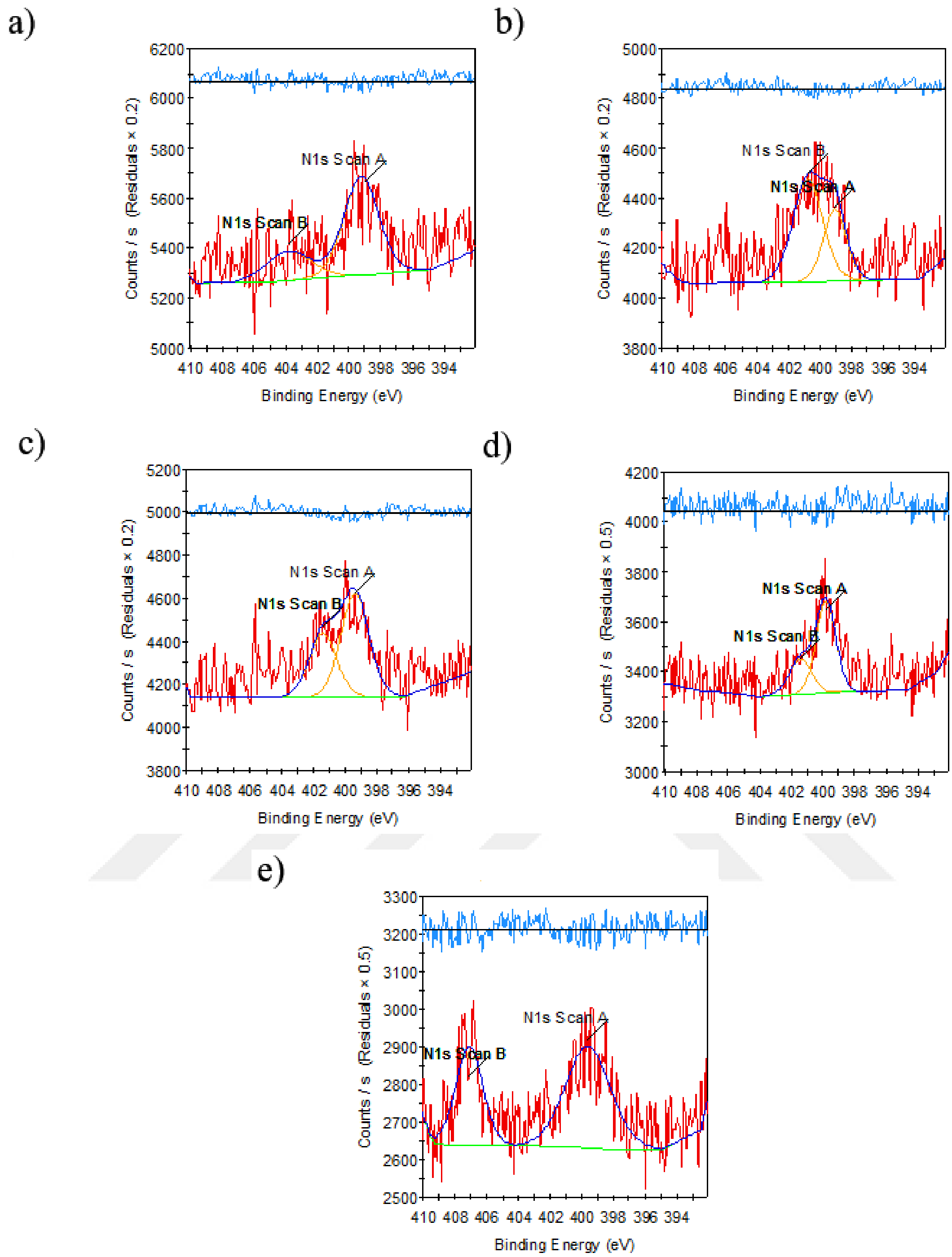

Figure 4. X-ray photoelectron spectroscopy N 1s scans of a) RGO-Pyr, b) PEG550, c) PEG2000, d) PEG5000 and e) RGO-Pyr-OD

In N1s XPS spectra, the peak locations at around 399 eV were attributed to the unfunctionalized nitrogen atom of the pyridine group. The second peak observed in RGO-Pyr spectra at 403.78 eV can be due to the oxidation of pyridinic nitrogen. For the other samples, the second peak was due to the PEG and octadecane attachment to pyridinic nitrogen, which causes a positive charge on the nitrogen atom. The ratio of positively charged pyridinic nitrogen to total pyridinic nitrogen was calculated using the areas under each peak. PEG550 showed the most successful pyridine grafting with a 0.65 ratio of PEGylated nitrogen to total nitrogen. Also, chains with higher molecular weight showed lower pyridine grafting ratios for PEGylated samples.

Table 2. Peak locations and the ratio of positively charged pyridinic nitrogen to total pyridinic nitrogen

Sample	Peak Location (eV)		PEGylated/octadecane attached N:Total N
RGO-Pyr	399.18	403.78	-
PEG550	399.08	400.78	0.65
PEG2000	399.38	401.38	0.38
PEG5000	399.78	401.48	0.30
RGO-Pyr-OD	399.68	407.08	0.36

In the elemental composition analysis for RGO-Pyr, 1.27 % nitrogen atom is present, whereas the atomic percentage of carbon is 66.13 %. By relating the percentages, 1 pyridine group is calculated to present approximately 52 carbon atoms of reduced graphene oxide. The ratio of carbon atoms per a single PEG or octadecane chain was then found by dividing the carbon number per pyridine group by the pyridine grafting ratio.

Table 3. The number of carbon atoms per PEG or octadecane chain

Sample	Number of carbon atoms per PEG or octadecane chain
PEG550	79
PEG2000	136
PEG5000	171
RGO-Pyr-OD	145

Table 4. The atomic percentages calculated from X-ray photoelectron spectroscopy data

	Atomic %				
Compound	RGO-Pyr	PEG550	PEG2000	PEG5000	RGO-Pyr-OD
C 1s	66.13	61.14	51.43	68.00	58.32
O 1s	17.97	22.8	27.44	17.79	22.38
N 1s	1.27	0.72	1.00	1.05	1.75
Si 2p	1.56	1.31	1.09	1.36	-
Na 1s	0.74	1.74	5.71	0.45	7.18
S 2p	-	0.71	3.10	-	-
Cl 2p	-	0.87	-	0.24	-

Zeta potential is an analysis method for determining the stability of particles inside a dispersion. Zeta potential also suggests the charge of the dispersed particle. When a charged surface is surrounded by solvent, the ions with an opposite charge firmly attached to the surface form a layer called Stern layer[35]. Outside the Stern layer, another layer consists of ions with both charges and is loosely attached to the surface. The boundary of this layer is called the slipping plane. Outside the slipping plane, ions of the dispersion medium are assumed free of interactions with the charged surface. The electrical potential of the charged surface at the slipping plane of the electrical double layer is called zeta potential. Zeta potential gives the potential difference between the charged particle and the bulk fluid[36]. High zeta potential values, positive or negative, suggest the dispersed system's stability since it means the electrostatic repulsion between the particles prevents coagulation. Particles with lower zeta potential tend to coagulate more quickly since they lack strong repulsive forces between them. Dispersion with particles having higher zeta potential than +30 mV or -30 mV is considered stable, whereas stability decreases as zeta potential values of particles get lower[37].

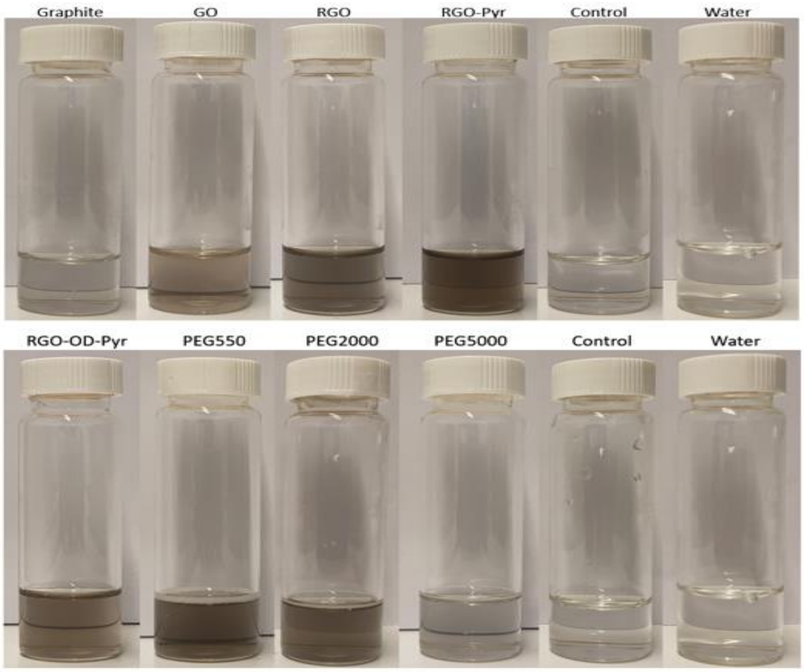

Figure 5. Stable parts of the sample dispersions taken after 2 hours of sonication and 30 minutes of the settling period

To determine the zeta potential of particle, the sample is subjected to an electric field. The mobility of the particle inside the solution due to the applied electric field is measured with the Doppler effect[38]. A laser beam is introduced into the solution, and the light's scattering due to particles causes a shift in the light frequency. The shift in frequency is then converted into particle speed using the Doppler effect and then to zeta potential by Henry or Smolochuski approximations[39].

The Zeta potential of particles is decreased after PEGylation because PEG is a neutral and non-absorbent polymer. PEG chains can extend beyond the electrical double layer and lower the ion concentration at the slipping plane due to its steric exclusion mechanism. This mechanism causes ion concentration at the slipping plane to drop and causes lower zeta potential values than expected. The reduction of zeta potential is correlated with the density of PEG coverage at the particle surface, with denser PEG coverage resulting in more reduction of zeta potential[40].

The zeta potential of all the samples was negative, suggesting a negative surface charge. From zeta potential values, we can say that RGO is moderately stable since it has a zeta potential of around -21,88 mV. After pyridine functionalization, the absolute value of zeta potential was increased to -28 mV, indicating increased stability. This change can be attributed to the reduced size RGO-Pyr compared to RGO. RGO-Pyr having less particle size showed higher electrophoretic mobility than bigger RGO particles inside the dispersion. As expected, PEGylation with 550 da molecular weight and 2000 da molecular weight decreased zeta potential to -11 mV and -16 mV relatively due to the steric exclusion effect lowering the ion concentration at the slipping plane. The decrease in zeta potential after octadecane addition can be attributed to a similar effect with PEG since both octadecane and PEG are neutral polymer chains capable of steric exclusion. We also observed increasing zeta potential due to the increasing molecular weight of PEG. This effect can be attributed to PEG with higher molecular weight having lower coverage at the surface, causing a lower reduction effect on zeta potential.

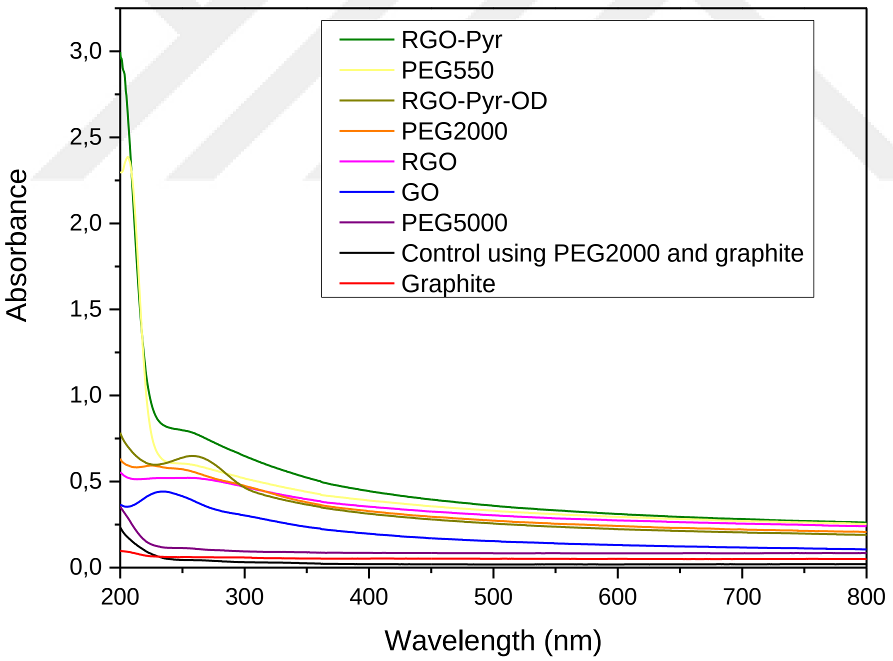

Figure 6. Ultraviolet-visible light spectroscopy results of samples

Ultraviolet-visible (UV-Vis) spectroscopy is widely used for the quantitative analysis of compounds. Uv-Vis produces light with wavelengths near UV (180-390 nm) or visible (380-780nm) and detects the absorbance of the sample at each wavelength [41]. When the light at the ultraviolet or visible range passes through a sample, specific wavelengths are absorbed due to π electrons or non-bonding electrons[42]. Therefore, using Lambert-Beer's law, it is possible to obtain a sample concentration according to its absorbance at a certain wavelength.

According to Lambert-Beer's law, the relation between absorbance and concentration is given by:

$$A = \log_{10}(I_0/I) = \varepsilon c L$$

Where A is the absorbance measured by the equipment, I_0 is the incident light intensity, I is the transmitted light intensity, ε is the molar absorptivity coefficient specific for each material, c is the sample concentration, and L is the length at which light passes through the sample[43]. The molar absorptivity coefficient of the graphene at 660 nm was found to be 2.460 $Lg^{-1}m^{-1}$. Suppose the wavelength of incident light is known. In that case, it is possible to calculate the concentration of a graphene dispersion sample using the given molar absorptivity coefficient and measured absorbance value[44].

Table 5. Concentrations of sample dispersions calculated using Lambert-Beer's law

Sample	**Concentration (µg/mL)**
Graphite	2.03
GO	4.95
RGO	10.69
RGO-Pyr	11.86
PEG550	11.38
PEG2000	9.30
PEG5000	3.41
RGO-Pyr-OD	8.61
Control using graphite and PEG2000	0.77

The dispersion stability of a material in the solvent is affected by its polarity. Generally, polar compounds are better dispersed in polar solvents and vice versa. Graphite having C-C bonds shows a non-polar characteristic. In contrast, hydroxyl, epoxy and carboxy introduced intro graphite by oxidation increasing polarity and made it suitable for interacting with non-polar solvents[45]. Therefore, the oxidation of graphite increases its dispersion stability in non-polar solvents such as water.

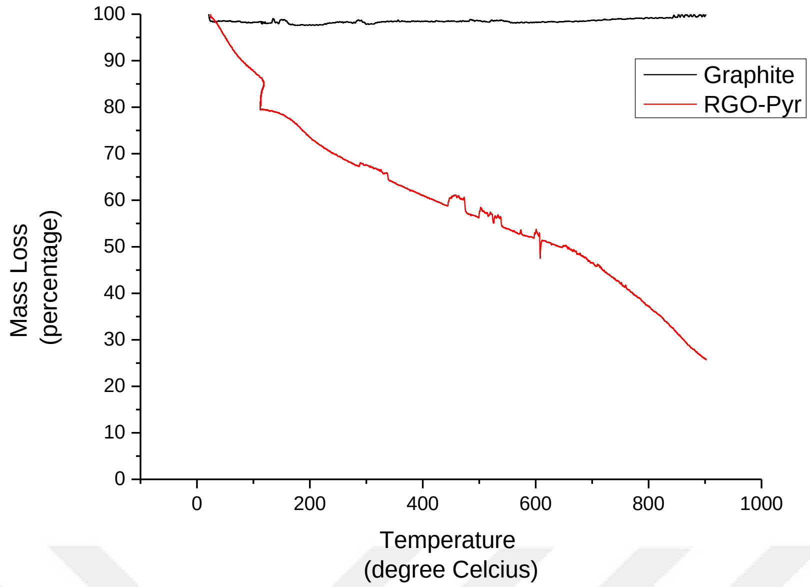

Figure 7. Thermogravimetric profiles of RGO-Pyr and pure graphite

Concentrations of the staple parts of the dispersion taken after 30 minutes of resting were calculated from UV-Vis spectra. GO showed higher concentration graphite indicating better dispersion stability due to added functional groups during oxidation. Pyridine attachment to RGO can have two possible effects on dispersion stability. Firstly, a decrease in dispersion quality due to increased density of the RGO after pyridine addition causes sedimentation. Secondly, smaller particle size and higher surface area of RGO-Pyr, when compared to RGO, cause more effective electrical double layer repulsive forces, increasing the dispersion stability. The concentrations obtained from UV-Vis suggest that these two effects almost cancel each other since the concentration of RGO and RGO-Pyr only differ by 10 %.

Similarly, adding PEG to RGO-Pyr causes steric stabilization, which increases dispersion stability and density. Therefore, the reduced concentration of the samples at increasing PEG molecular weight can be attributed to the effect of density overcoming steric stabilization. Despite having a lower molecular weight than PEG550 and PEG2000, the octadecane chain did not cause an increase in concentration which can be attributed to the lower steric stabilization of the octadecane chain compared to PEG chains.

Thermogravimetric analysis is a tool utilized for determining the response of nanomaterials or polymer composites under heating[46]. Under controlled heating rate and atmosphere, the weight loss of the sample is determined related to time or temperature[47]. A thermogravimetric analyzer consists of a programmable furnace for a controlled heating rate. This isolated chamber prevents additional heat effects and provides a controlled atmosphere and a sensitive balance inside the chamber for continuous weight measurement[48].

The decomposition of pyridine starts at around 330 ℃ and ends until 600 ℃. In the mass loss profile of RGO-Pyr, the mass loss between 330 ℃-600 ℃ is 14,04 %. The thermogravimetric profile of pure graphite showed 1,69 % mass loss at 600 ℃. Comparing mass loss percentages of graphite and RGO-Pyr between 330 ℃-600 ℃, and molecular weights of carbon and pyridine group, 1 pyridine group is calculated present per 53 carbon atoms. The result is in close agreement with the XPS calculations, which showed 1 pyridine group per 52 carbon atoms of reduced graphene oxide.

Polarized light microscopy is a characterization technique widely utilized for imaging protein crystals. Polarized light is an electromagnetic wave whose electric field vectors vibrate in a single plane as opposed to other sources of light whose electric field vectors vibrate in all planes. Polarization of light is achieved by passing light into a medium that restricts its vibration in specific planes. A polarized light microscope consists of an illuminator that produces unpolarized light, a polarizer that restricts unpolarized light's vibration to single-plane vibration, and an analyzer to absorb the transmitted polarized light[49]. Polarized light microscopy is especially useful for determining protein crystals since some proteins show birefringence[50]. The refractive indexes of the birefringent materials vary according to the polarization of the light[51]. Upon passing through a birefringent sample, polarized light is divided into faster and slower travelling components, which emerge from the material with a phase difference. The phase difference is detected as a glow-on image making protein crystals easier to see. Crystal growth in the droplets containing protein, buffer solution and nucleants was evaluated each day under the polarized light microscope.

An essential parameter for the effectiveness of a nucleant is its ability to reduce crystal formation time. Nucleants that form a strong attraction with protein molecules reduce the time required for the first crystal to grow by increasing the protein concentration. Droplets containing nucleant samples showed crystal growth in the first 24 hours, except the droplet containing PEG2000, which produced crystal on the third day. Control samples containing only buffer solution and protein showed crystal growth on the fourth day. All of the samples tested decreased the time required for the first crystal to appear compared to the control suggesting successful interactions with lysozyme. The difference in time for RGO, RGO-Pyr, PEG550, PEG5000 and RGO-Pyr-OD is three days, whereas, for PEG2000, it is one day.

Table 6. Crystal Formation percentage of hanging drop kits prepared

Day	Percentage of Droplets with Crystal Formation (%)						
	RGO	RGO-Pyr	PEG550	PEG2000	PEG5000	RGO-Pyr-OD	Control
1	66	33	33	0	50	66	0
2	66	33	33	0	50	66	0
3	100	33	33	33	50	66	0
4	100	100	66	66	50	100	33
5	100	100	66	66	50	100	33

Polarized light microscope images show lysozyme crystals appearing in a different colour from their medium. The colour difference between a crystal and its medium signifies its diffraction quality. All of the tested samples, including the control, were able to produce crystals of a different colour than their medium indicating good diffraction quality. In the first 24 hours, crystals formation occurs except for PEG2000 and control. However, in the images of the fifth-day, distortion of crystals in the droplets containing RGO-Pyr, PEG550, PEG5000 and RGO-Pyr-OD is observed. For PEG550, PEG5000 and RGO-Pyr-OD, this can be due to the electrostatic interaction between the positively charged pyridine and negatively charged lysozyme molecules at the crystal surface, pulling lysozyme molecules out of the crystal lattice. For RGO-Pyr same effect can be attributed to the covalent bonding of the pyridine atom with the sulphur atom of cysteine amino acid included in lysozyme.

Another parameter to assess the effectiveness of a nucleant is to look at the number of droplets with crystal growth. RGO and RGO-Pyr-OD produced crystals in two of three kits tested on the first day. Crystallization in all the kits reached the quickest for RGO on the third day, whereas for RGO-Pyr-OD, all kits showed crystal growth on the fourth day. For RGO-Pyr and PEG550, two out of three kits produced crystals on the first day. All of the kits containing RGO-Pyr showed crystal growth on the fourth day. For PEG550 and PEG2000, only two out of three kits were able to produce crystals during five days period, whereas PEG5000 showed crystal growth in one of the two droplets during the same period.

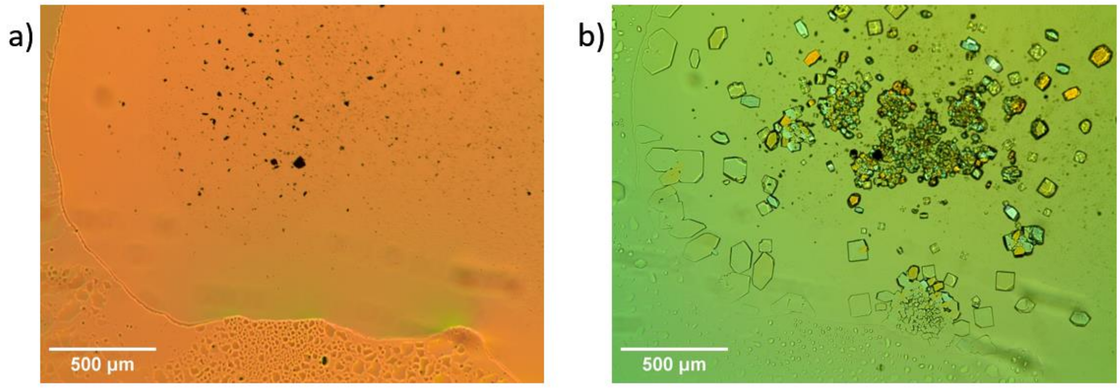

Figure 8. Polarized light microscope images of droplets containing RGO-Pyr as the nucleant taken from the same area of the droplet at a) right after preparation and b) after 12 days

In the polarized light microscope images, nucleant samples are seen as black dots inside the droplet. In figure 8, the crystals on the 12th day are grown at two locations: the droplet boundary and the area that is concentrated with nucleant. This suggests that the crystallization process can occur at the nucleant surface, and nucleant samples act as foreign surfaces like droplet boundaries that induce heterogeneous nucleation.

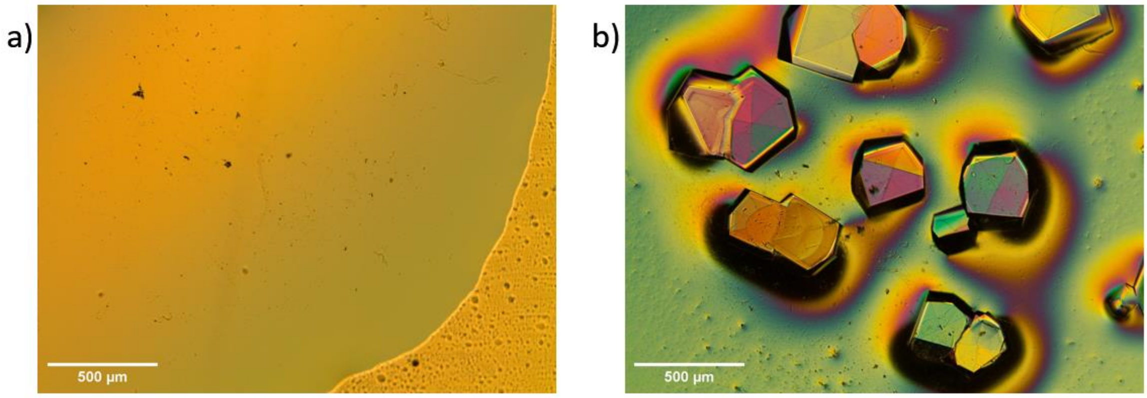

Figure 9. Polarized light microscope images of droplets containing RGO as the nucleant taken a) right after preparation and b) after 5 days

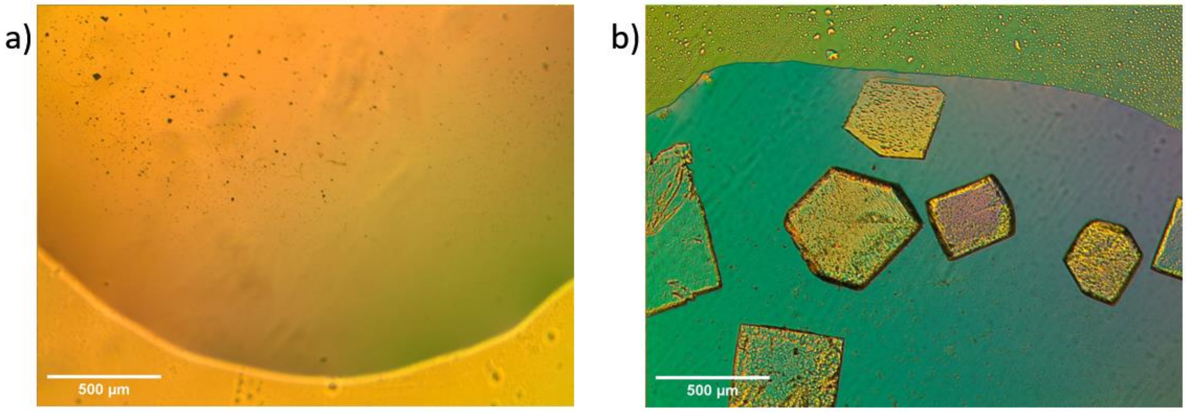

Figure 10. Polarized light microscope images of droplets containing RGO-OD as the nucleant taken a) right after preparation and b) after 5 days

RGO showed the highest average number of crystals per droplet on the first day and after 5 days. Also, considering the faster growth of crystals for droplets containing RGO samples, the crystallization effect of RGO can be attributed to the pi-pi interactions and hydrophobic interactions between lysozyme and RGO surface. It was shown that additional functional groups to the graphene surface decrease the availability of the surface to other molecules. Because both PEG and octadecane are long carbon chains, they can cause steric exclusion to lysozyme molecules and prevent adsorption to the RGO surface. This negative effect on protein crystallization can nullify the positive effect of added functional groups. Because RGO has performed better as a nucleant than PEGylated samples with functional groups, it can be suggested that the pi-pi interaction and hydrophobic interaction from the RGO surface on protein crystallization are greater than the effect from functional groups. For example, the depletion mechanism of PEG and positive charge on pyridine and lone electron pair of the nitrogen atom of pyridine resulted in better crystallization for RGO-Pyr, PEG550 and PEG2000 compared to the control sample with no nucleants. But except for RGO-Pyr-OD, samples with added residues performed less than RGO even though having functional groups that can interact with lysozyme.

Table 7. Numbers and sizes of the crystals

	Average Number of Crystals per Droplet		Average Crystal Size (µm)	
Sample	Day 1	Day 5	Day 1	Day 5
RGO	15.67 ± 1.28	22.67 ± 7.31	261.48 ± 87.29	234.90 ± 112.70
RGO-Pyr	2.67 ± 3.77	11.00 ± 4.96	317.42 ± 108.25	130.39 ± 162.92
PEG550	2.67 ± 3.77	3.33 ± 3.39	271.69 ± 78.39	277.25 ± 113.12
PEG2000	0	1.67 ± 1.24	0	65.02 ± 24.28
PEG5000	3.50 ± 3.50	3.50 ± 3.50	266.00± 77.31	228.71 ± 80.15
RGO-Pyr-OD	10.00 ± 7.48	10.33 ± 4.92	425.28 ± 99.71	315.80 ± 127.05
Control	0	3.66 ± 2.35	0	91.36 ± 41.99

The largest average crystal size was observed for the droplets containing RGO-Pyr-OD. The crystallization effect of RGO-Pyr-OD is due to the combined impact of hydrophobic and pi-pi attraction between RGO and lysozyme, the positive charge of pyridine and the hydrophobic interactions between octadecane and lysozyme. The smaller molecular weight of octadecane compared to PEG can also facilitate the more accessible electrostatic attraction of lysozyme with the positive charge of pyridine because a smaller chain weight reduces the effect of steric exclusion, which keeps lysozyme away from the surface. The crystal number and size in droplets containing RGO-Pyr were higher compared to PEGylated samples. This can be because of the lone electron pair of pyridine forming hydrogen bonds with lysozyme creating a more significant effect on crystallization than the depletion mechanism of PEG. PEG2000 showed the smallest number of crystals and the smallest crystal size on the 5th day. This can be due to the molecular weight of the PEG chain. In the literature, the PEG with the higher molecular weight is shown to have a higher depletion potential that induces protein crystallization[52]. Since 2000 da is a lower molecular weight and less crystal size, and the number of PEG2000 compared to PEG5000 agrees with the literature. PEG550, despite having the lowest PEG molecular weight, showed the highest number of crystals and largest crystal sizes. This can be attributed to the short chain of PEG550 creating less steric exclusion, preventing protein molecules from adsorbing onto the graphene surface than other PEGylated samples.

2.5 Conclusions

In this thesis, we have developed novel pyridine and PEG functionalized graphene nucleants for protein crystallization. Six samples were tested as nucleants for lysozyme crystallization: RGO, RGO-Pyr, PEG550, PEG2000, PEG5000 and RGO-Pyr-OD. The increased D band confirmed the successful reduction of RGO from GO in the Raman spectra of RGO compared to the Raman spectra of GO. Particle size decreased after pyridine addition to RGO, indicating the columbic repulsive force of pyridine electrons separating graphene layers apart. After PEGylation and octadecane grafting, increases in particle size due to additional long chains were observed. Pyridine functionalized also increased the magnitude of zeta potential. This change was attributed to a decreased particle size of RGO-Pyr, causing higher electrophoretic mobility. After PEGylation, the magnitude of zeta potential dropped because of the extending PEG chains beyond the electrical double layer, causing the slipping plane to be pushed further away from the surface. Mass loss calculated from the thermogravimetric analysis is used for calculating the grafting ratio. Octadecane having a lower molecular weight than PEG molecules, showed the most efficient carbon-to-grafted molecule ratio, followed by PEG550. Higher grafting was observed for PEG2000 and PEG5000 due to their higher molecular weight. Polarized light microscope images showed crystals with good diffraction quality obtained in all samples. Distortion on the crystal surface was observed in droplets containing RGO-Pyr, PEG550, PEG5000 and RGO-Pyr-OD. This was attributed to the electrostatic attraction forces between negatively charged lysozyme and positively charged pyridine atoms in PEG550, PEG5000 and RGO-Pyr-OD pulling lysozyme molecules at the crystal surface. For RGO-Pyr, the same phenomenon was explained as possible hydrogen bonds between the nitrogen atom of pyridine containing lone electron pair and lysozyme molecule overcoming weak electrostatic forces that form the lysozyme crystal.

All of the samples except PEG2000 were able to produce crystals in the first 24 hours, whereas control droplets without any nucleant did not show significant crystal growth until the fourth day. The lowest number of crystals and smallest crystal size was observed for droplets containing PEG2000. This was attributed to a lower grafting ratio of PEG2000 compared to other PEGylated samples and RGO-Pyr-OD. RGO produced the highest number of crystals with an average size of 221 µm. The crystallization effect of RGO is only due to hydrophobic and pi-pi interactions between the RGO surface and lysozyme. It was shown in the literature that additional functional groups decrease the surface availability of graphene. Having no functional groups, the surface of RGO is unhindered by steric exclusion of added functionalized groups that prevent protein adsorption onto the surface. However, all the other samples contain functional groups indicating possible passivation of the surface of RGO. RGO without any functional group having a higher number and bigger size of crystals than RGO-Pyr and PEGylated samples suggest a dominating impact of hydrophobic interactions and pi-pi interactions over hydrogen bonding of RGO-Pyr and the combination of depletion mechanism of PEGylated samples or hydrophobic effect of octadecane chain with a positive charge of pyridine. RGO-Pyr performed better than PEGylated samples on crystal size and number, suggesting a hydrogen bonding between the nitrogen atom of pyridine containing electron pair and lysozyme. Hydrogen bonding created a stronger attraction force for lysozyme crystallization than the electrostatic interaction and depletion mechanism provided by PEGylated samples resulting in more and bigger crystal growth in droplets containing RGO-Pyr than in PEGylated samples. The biggest crystals were observed in RGO-Pyr-OD. This can be due to the lower molecular weight of octadecane creating less steric exclusion than tested PEG chains, allowing more accessible RGO surface and easier electrostatic interactions between positively charged pyridine and negatively charged lysozyme. Having the biggest crystal size and higher number of crystals produced than PEGylated samples, RGO-Pyr-OD shows promising potential as a novel nucleant for protein crystallization.

REFERENCES

(1) Sun, P. D., Foster, C. E., & Boyington, J. C. (2004). Overview of protein structural and functional folds. In *Current protocols in protein science / editorial board, John E. Coligan ... [et al.]: Vol. Chapter 17*. https://doi.org/10.1002/0471140864.ps1701s35

(2) Kubiak-Ossowska, K., & Mulheran, P. A. (2010). Mechanism of hen egg white lysozyme adsorption on a charged solid surface. *Langmuir*, *26*(20), 15954–15965. https://doi.org/10.1021/la102960m

(3) Bijelic, A., Molitor, C., Mauracher, S. G., Al-Oweini, R., Kortz, U., & Rompel, A. (2014). Hen egg-white lysozyme crystallization: Protein stacking and structure stability enhanced by a tellurium(VI)-centred polyoxotungstate. *ChemBioChem*, *16*(2), 233–241. https://doi.org/10.1002/cbic.201402597

(4) de Yoreo, J. J., & Vekilov, P. G. (n.d.). *Principles of Crystal Nucleation and Growth*.

(5) Chayen, N. E., Saridakis, E., El-Bahar, R., & Nemirovsky, Y. (2001). Porous silicon: An effective nucleation-inducing material for protein crystallization. *Journal of Molecular Biology*, *312*(4), 591–595. https://doi.org/10.1006/jmbi.2001.4995

(6) Rong, L., Komatsu, H., Yoshizaki, I., Kadowaki, A., & Yoda, S. (2004). Protein crystallization by using porous glass substrate. In *J. Synchrotron Rad* (Vol. 11).

(7) Yoshizaki, I., Sato, T., Igarashi, N., Natsuisaka, M., Tanaka, N., Komatsu, H., & Yoda, S. (2001). Biological Crystallography Systematic analysis of supersaturation and lysozyme crystal quality. *Acta Cryst*, *57*, 1621–1629.

(8) Nanev, C. N., Saridakis, E., & Chayen, N. E. (2017). Protein crystal nucleation in pores. *Scientific Reports*, *7*. https://doi.org/10.1038/srep35821

(9) Chayen, N. E., Saridakis, E., & Sear, R. P. (2006). *Experiment and theory for heterogeneous nucleation of protein crystals in a porous medium*. https://www.pnas.org

(10) Tanaka, S., & Ataka, M. (2002). Protein crystallization induced by polyethylene glycol: A model study using apoferritin. *Journal of Chemical Physics*, *117*(7), 3504–3510. https://doi.org/10.1063/1.1477456

(11) Vivarès, D., Belloni, L., Tardieu, A., & Bonneté, F. (2002). Catching the PEG-induced attractive interaction between proteins. *European Physical Journal E*, *9*(1), 15–25. https://doi.org/10.1140/epje/i2002-10047-7

(12) Sear, R. P. (2003). *Protein crystals and charged surfaces: interactions and heterogeneous nucleation*.

(13) Falini, G., Fermani, S., Conforti, G., & Ripamonti, A. (2002). Protein crystallization on chemically modified mica surfaces. In *Acta Cryst* (Vol. 58).

(14) Tosi, G., Fermani, S., Falini, G., Gavira Gallardo, J. A., & García Ruiz, J. M. (2008). Crystallization of proteins on functionalized surfaces. *Acta Crystallographica Section D: Biological Crystallography*, *64*(10), 1054–1061. https://doi.org/10.1107/S0907444908025079

(15) Rong, L., Komatsu, H., & Yoda, S. (2002). Control of heterogeneous nucleation of lysozyme crystals by using Poly-L-Lysine modified substrate. In *Journal of Crystal Growth* (Vol. 235).

(16) Chen, J., Xu, E., Wei, Y., Chen, M., Wei, T., & Zheng, S. (2022). Graph Clustering Analyses of Discontinuous Molecular Dynamics Simulations: Study of Lysozyme Adsorption on a Graphene Surface. *Langmuir*, *38*(35), 10817–10825. https://doi.org/10.1021/acs.langmuir.2c01331

(17) Bunyaev, V. A., Shnitko, A. v., Chernysheva, M. G., Ksenofontov, A. L., & Badun, G. A. (2022). Structural peculiarities of lysozyme-graphene oxide adsorption complexes. *Fullerenes Nanotubes and Carbon Nanostructures*, *30*(1), 99–105. https://doi.org/10.1080/1536383X.2021.1988574

(18) Gully, B. S., Zou, J., Cadby, G., Passon, D. M., Iyer, K. S., & Bond, C. S. (2012). Colloidal graphenes as heterogeneous additives to enhance protein crystal yield. *Nanoscale*, *4*(17), 5321–5324. https://doi.org/10.1039/c2nr31150j

(19) Asanithi, P., Saridakis, E., Govada, L., Jurewicz, I., Brunner, E. W., Ponnusamy, R., Cleaver, J. A. S., Dalton, A. B., Chayen, N. E., & Sear, R. P. (2009). Carbon-nanotube-based materials for protein crystallization. *ACS Applied Materials and Interfaces*, *1*(6), 1203–1210. https://doi.org/10.1021/am9000858

(20) Govada, L., Leese, H. S., Saridakis, E., Kassen, S., Chain, B., Khurshid, S., Menzel, R., Hu, S., Shaffer, M. S. P., & Chayen, N. E. (2016). Exploring Carbon Nanomaterial Diversity for Nucleation of Protein Crystals. *Scientific Reports*, *6*. https://doi.org/10.1038/srep20053

(21) Leese, H. S., Govada, L., Saridakis, E., Khurshid, S., Menzel, R., Morishita, T., Clancy, A. J., White, E. R., Chayen, N. E., & Shaffer, M. S. P. (2016). Reductively PEGylated carbon nanomaterials and their use to nucleate 3D protein crystals: A comparison of dimensionality. *Chemical Science*, *7*(4), 2916–2923. https://doi.org/10.1039/c5sc03595c

(22) Govada, L., Rubio, N., Saridakis, E., Balaskandan, K., Leese, H. S., Li, Y., Wang, B., Shaffer, M. S. P., & Chayen, N. (2022). Graphene-Based Nucleants for Protein Crystallization. *Advanced Functional Materials*, *32*(42). https://doi.org/10.1002/adfm.202202596

(23) Huang, X. D., Goh, S. H., & Lee, S. Y. (2000). Miscibility of C60-end-capped poly(ethylene oxide) with poly(p-vinylphenol). *Macromolecular Chemistry and Physics*, *201*(18), 2660–2665. https://doi.org/10.1002/1521-3935(20001201)201:18<2660::AID-MACP2660>3.0.CO;2-8

(24) Bayazit, M. K., Pålsson, L. O., & Coleman, K. S. (2015). Sensing properties of light-emitting single walled carbon nanotubes prepared via click chemistry of ylides bound to the nanotube surface. *RSC Advances*, *5*(46), 36865–36873. https://doi.org/10.1039/c5ra04330a

(25) Muehlethaler, C., Gueissaz, L., & Massonnet, G. (2013). Forensic Paint Analysis. In *Encyclopedia of Forensic Sciences: Second Edition* (pp. 265–272). Elsevier Inc. https://doi.org/10.1016/B978-0-12-382165-2.00109-4

(26) Adya, A. K., & Canetta, E. (2013). Nanotechnology and Its Applications to Animal Biotechnology. In *Animal Biotechnology: Models in Discovery and Translation* (pp. 247–263). Elsevier Inc. https://doi.org/10.1016/B978-0-12-416002-6.00014-6

(27) Muzyka, R., Drewniak, S., Pustelny, T., Chrubasik, M., & Gryglewicz, G. (2018). Characterization of graphite oxide and reduced graphene oxide obtained from different graphite precursors and oxidized by different methods using Raman spectroscopy. *Materials*, *11*(7). https://doi.org/10.3390/ma11071050

(28) Englert, J. M., Vecera, P., Knirsch, K. C., Schäfer, R. A., Hauke, F., & Hirsch, A. (2013). Scanning-Raman-microscopy for the statistical analysis of covalently functionalized graphene. *ACS Nano*, *7*(6), 5472–5482. https://doi.org/10.1021/nn401481h

(29) Kudin, K. N., Ozbas, B., Schniepp, H. C., Prud'homme, R. K., Aksay, I. A., & Car, R. (2008). Raman spectra of graphite oxide and functionalized graphene sheets. *Nano Letters*, *8*(1), 36–41. https://doi.org/10.1021/nl071822y

(30) Hidayah, N. M. S., Liu, W. W., Lai, C. W., Noriman, N. Z., Khe, C. S., Hashim, U., & Lee, H. C. (2017). Comparison on graphite, graphene oxide and reduced graphene oxide: Synthesis and characterization. *AIP Conference Proceedings*, *1892*. https://doi.org/10.1063/1.5005764

(31) Raval, N., Maheshwari, R., Kalyane, D., Youngren-Ortiz, S. R., Chougule, M. B., & Tekade, R. K. (2018). Importance of physicochemical characterization of nanoparticles in pharmaceutical product development. In *Basic Fundamentals of Drug Delivery* (pp. 369–400). Elsevier. https://doi.org/10.1016/B978-0-12-817909-3.00010-8

(32) Edward, J. T. (n.d.). *Molecular Volumes and the Stokes-Einstein Equation*. https://pubs.acs.org/sharingguidelines

(33) You, X., Chang, J. H., Ju, B. K., & Pak, J. J. (2011). An electrochemical route to graphene oxide. *Journal of Nanoscience and Nanotechnology*, *11*(7), 5965–5968. https://doi.org/10.1166/jnn.2011.4451

(34) Suhaimin, N. S., Hanifah, M. F. R., Jusin, J. wani, Jaafar, J., Aziz, M., Ismail, A. F., Othman, M. H. D., Abd Rahman, M., Aziz, F., Yusof, N., & Mohamud, R. (2021). Tuning the oxygen functional groups in graphene oxide nanosheets by optimizing the oxidation time. *Physica E: Low-Dimensional Systems and Nanostructures*, *131*. https://doi.org/10.1016/j.physe.2021.114727

(35) Shnoudeh, A. J., Hamad, I., Abdo, R. W., Qadumii, L., Jaber, A. Y., Surchi, H. S., & Alkelany, S. Z. (2019). Synthesis, Characterization, and Applications of Metal Nanoparticles. In *Biomaterials and Bionanotechnology* (pp. 527–612). Elsevier. https://doi.org/10.1016/B978-0-12-814427-5.00015-9

(36) Selvamani, V. (2018). Stability Studies on Nanomaterials Used in Drugs. In *Characterization and Biology of Nanomaterials for Drug Delivery: Nanoscience and Nanotechnology in Drug Delivery* (pp. 425–444). Elsevier. https://doi.org/10.1016/B978-0-12-814031-4.00015-5

(37) Joseph, E., & Singhvi, G. (2019). Multifunctional nanocrystals for cancer therapy: A potential nanocarrier. In *Nanomaterials for Drug Delivery and Therapy* (pp. 91–116). Elsevier. https://doi.org/10.1016/B978-0-12-816505-8.00007-2

(38) Watters, R. J., Kester, M., Tran, M. A., Loughran, T. P., & Liu, X. (2012). Development and use of ceramide nanoliposomes in cancer. In *Methods in Enzymology* (Vol. 508, pp. 89–108). Academic Press Inc. https://doi.org/10.1016/B978-0-12-391860-4.00005-7

(39) Kaszuba, M., Corbett, J., Watson, F. M. N., & Jones, A. (2010). High-concentration zeta potential measurements using light-scattering techniques. *Philosophical Transactions of the Royal Society A: Mathematical, Physical and Engineering Sciences*, *368*(1927), 4439–4451. https://doi.org/10.1098/rsta.2010.0175

(40) Rabanel, J. M., Hildgen, P., & Banquy, X. (2014). Assessment of PEG on polymeric particles surface, a key step in drug carrier translation. In *Journal of Controlled Release* (Vol. 185, Issue 1, pp. 71–87). Elsevier. https://doi.org/10.1016/j.jconrel.2014.04.017

(41) Worsfold, P. J. (2019). Spectrophotometry | overview. In *Encyclopedia of Analytical Science* (pp. 244–248). Elsevier. https://doi.org/10.1016/B978-0-12-409547-2.14265-9

(42) Wang, H., & Chu, P. K. (2013). Surface Characterization of Biomaterials. In *Characterization of Biomaterials* (pp. 105–174). Elsevier Inc. https://doi.org/10.1016/B978-0-12-415800-9.00004-8

(43) Dyamenahalli, K., Famili, A., & Shandas, R. (2015). Characterization of shape-memory polymers for biomedical applications. In *Shape Memory Polymers for Biomedical Applications* (pp. 35–63). Elsevier Ltd. https://doi.org/10.1016/B978-0-85709-698-2.00003-9

(44) Hernandez, Y., Nicolosi, V., Lotya, M., Blighe, F. M., Sun, Z., De, S., McGovern, I. T., Holland, B., Byrne, M., Gun'ko, Y. K., Boland, J. J., Niraj, P., Duesberg, G., Krishnamurthy, S., Goodhue, R., Hutchison, J., Scardaci, V., Ferrari, A. C., & Coleman, J. N. (2008). High-yield production of graphene by liquid-phase exfoliation of graphite. *Nature Nanotechnology*, *3*(9), 563–568. https://doi.org/10.1038/nnano.2008.215

(45) Oliveira, A. E. F., Braga, G. B., Tarley, C. R. T., & Pereira, A. C. (2018). Thermally reduced graphene oxide: synthesis, studies and characterization. *Journal of Materials Science*, *53*(17), 12005–12015. https://doi.org/10.1007/s10853-018-2473-3

(46) Loganathan, S., Valapa, B.R., Mishra, R., Pugazhenthi, G., Thomas, S. (2017). Thermogravimetry analysis ofr chrachterization of nanomaterials. In S. Thomas, R. Thomas, A. Zachariah & R. Mishra (Eds.). *Thermal and Rheological Measurement Techniques for Nanomaterials Characterization*. https://doi.org/10.1016/B978-0-323-46139-9.12001-8

(47) Inan, T. Y. (2017). Thermoplastic-based nanoblends: Preparation and characterizations. In *Recent Developments in Polymer Macro, Micro and Nano Blends: Preparation and Characterisation* (pp. 17–56). Elsevier Inc. https://doi.org/10.1016/B978-0-08-100408-1.00002-9

(48) Muehlethaler, C., Gueissaz, L., & Massonnet, G. (2013). Forensic Paint Analysis. In *Encyclopedia of Forensic Sciences: Second Edition* (pp. 265–272). Elsevier Inc. https://doi.org/10.1016/B978-0-12-382165-2.00109-4

(49) Koike-Tani, M., Tani, T., Mehta, S. B., Verma, A., & Oldenbourg, R. (2015). Polarized light microscopy in reproductive and developmental biology. In *Molecular Reproduction and Development* (Vol. 82, Issues 7–8, pp. 548–562). John Wiley and Sons Inc. https://doi.org/10.1002/mrd.22221

(50) Calero, G., Cohen, A. E., Luft, J. R., Newman, J., & Snell, E. H. (2014). Identifying, studying and making good use of macromolecular crystals. *Acta Crystallographica Section F:Structural Biology Communications*, *70*(8), 993–1008. https://doi.org/10.1107/S2053230X14016574

(51) Echalier, A., Glazer, R. L., Fülöp, V., & Geday, M. A. (2004). Assessing crystallization droplets using birefringence. *Acta Crystallographica Section D: Biological Crystallography*, *60*(4), 696–702. https://doi.org/10.1107/S0907444904003154

(52) Tanaka, S., Ataka, M., Onuma, K., & Kubota, T. (2003). Rationalization of membrane protein crystallization with polyethylene glycol using a simple depletion model. *Biophysical Journal*, *84*(5), 3299–3306. https://doi.org/10.1016/S0006-3495(03)70054-X

Supporting Information

In this study, four different hanging drop kits were prepared and named Kit 1, Kit 2, Kit 3 and Kit. The first three kits (Kit 1, Kit 2 and Kit 3) were prepared as described in the experimental section. Kit 4 was prepared using the method, except it does not include protein concentration. To be precise, Kit 4 contains nucleant solution of 0.5 µL and crystallization condition (Na buffer at 4.7 pH without any lysozyme) of 1.5 µL, making the total volume of droplet 2 µL. The volume of the crystallization condition at the reservoir was kept the same with the first three kits at 800 µL. The first three kits' crystals could be a protein or Na crystals. Therefore Kit 4 was prepared to test the crystallization of Na. Having no crystal growth at Kit 4, the crystals in the first three kits can be attributed to lysozyme since the nucleants tested showed no Na crystal growth.

Polarized light microscope images of every kit were captured right after the preparation. Afterwards, the same analysis was continued every day for every kit for 12 days. All of the images taken are given here as supporting information.

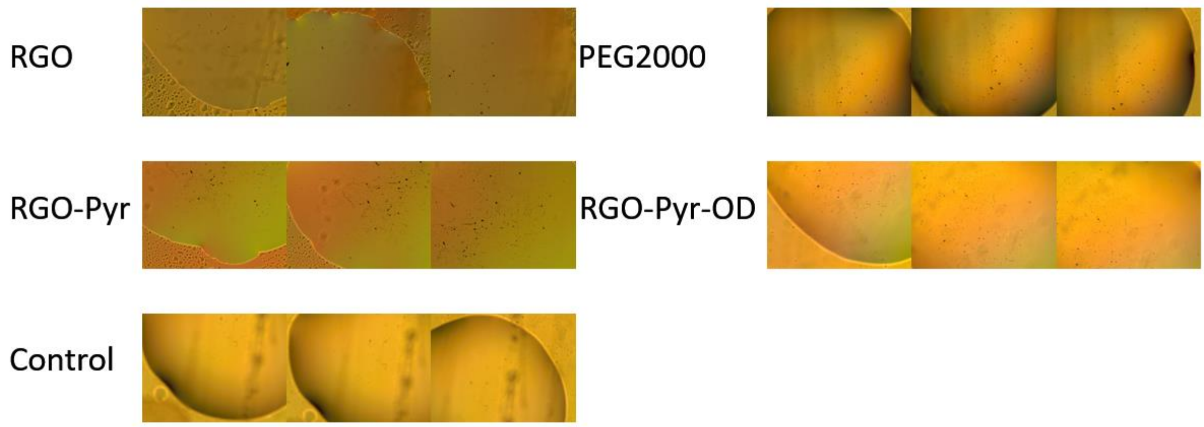

Supporting Figure 1. Polarized light microscope images of Kit 1 after preparation

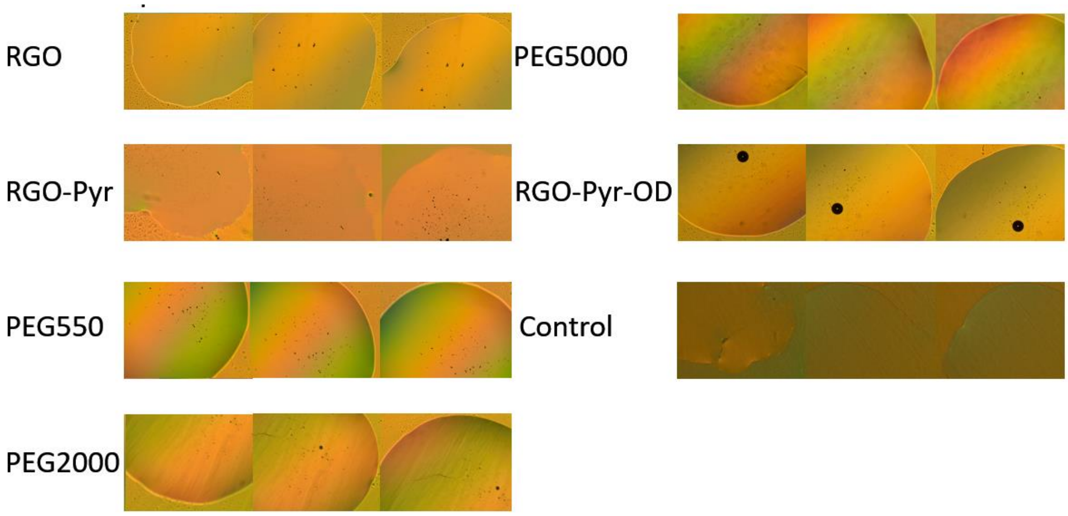

Supporting Figure 2. Polarized light microscope images of Kit 2 after preparation

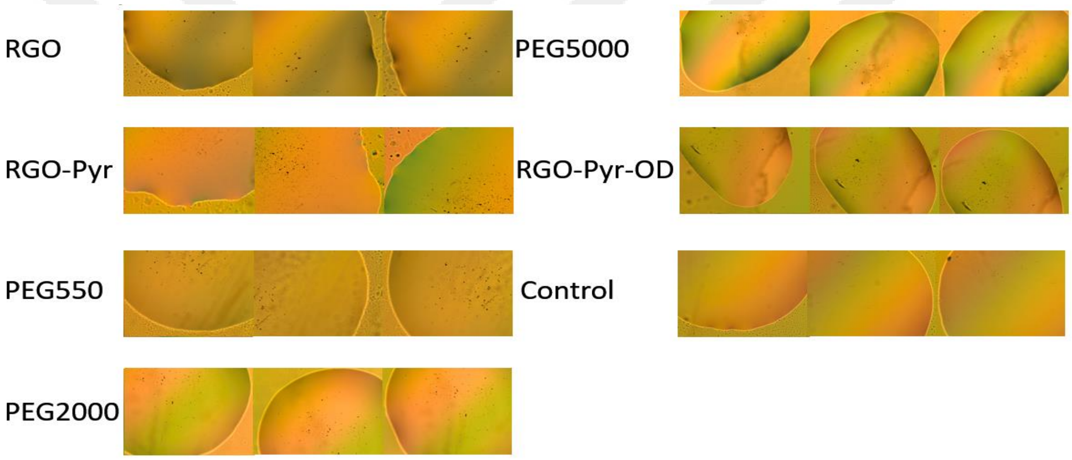

Supporting Figure 3. Polarized light microscope images of Kit 3 after preparation

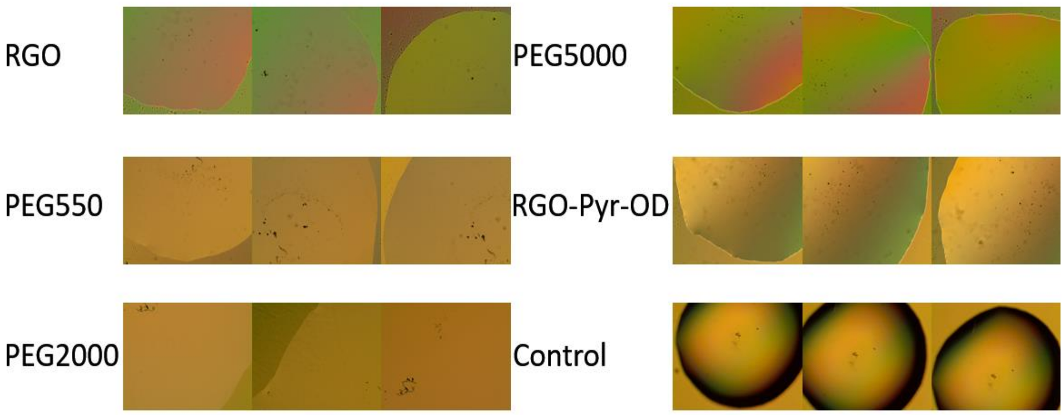

Supporting Figure 4. Polarized light microscope images of Kit 4 after preparation

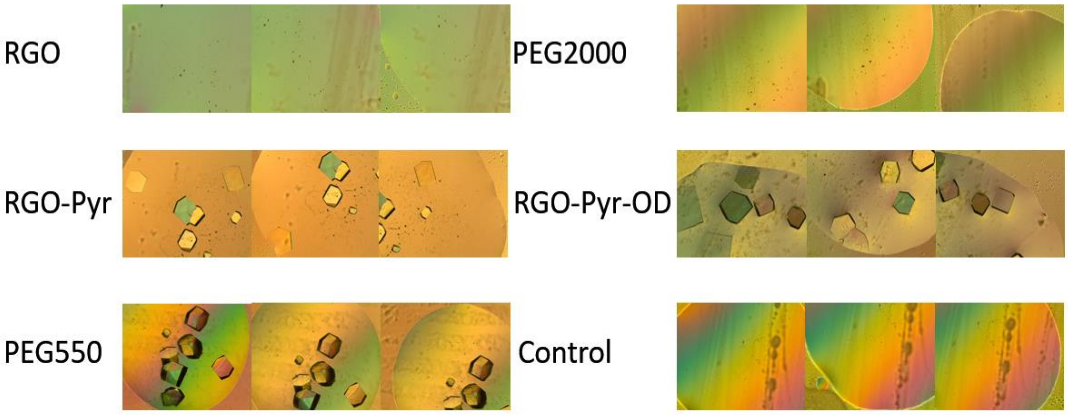

Supporting Figure 5. Polarized light microscope images of Kit 1 on the first day

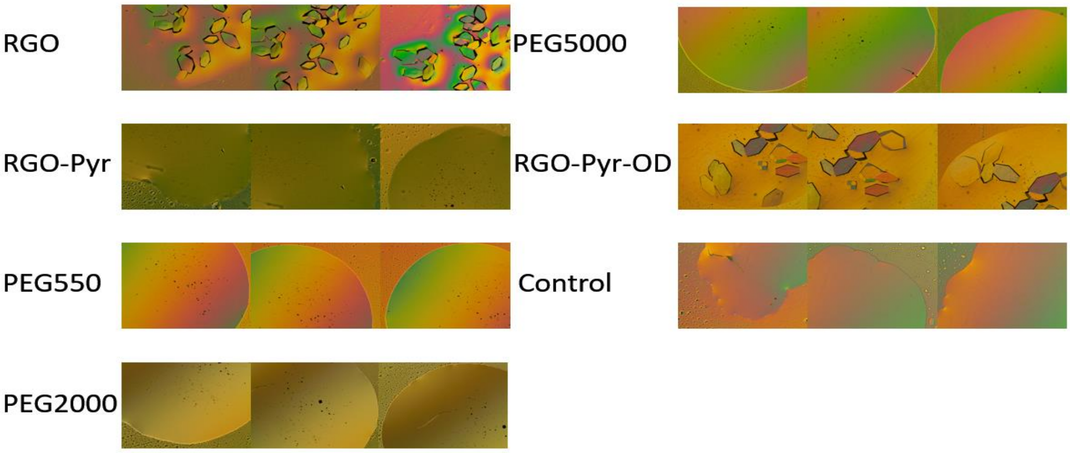

Supporting Figure 6. Polarized light microscope images of Kit 2 on the first day

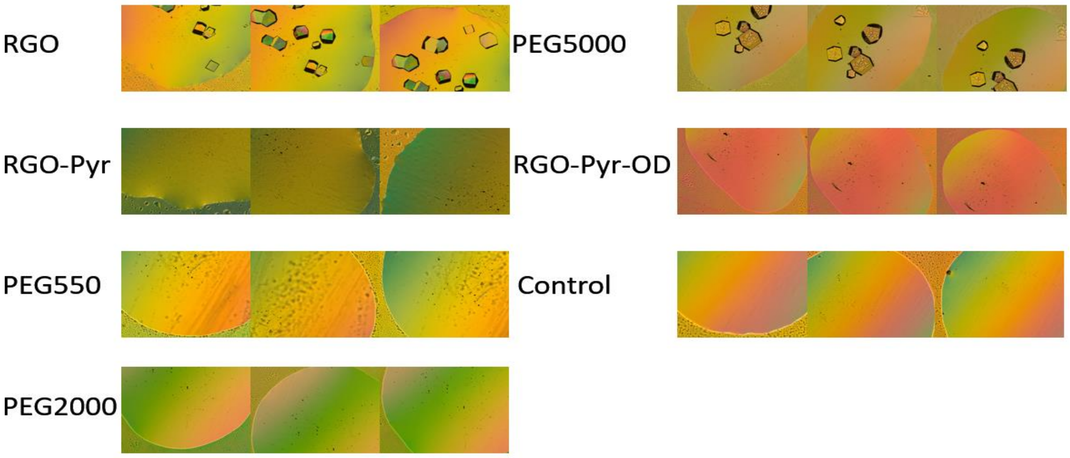

Supporting Figure 7. Polarized light microscope images of Kit 3 on the first day

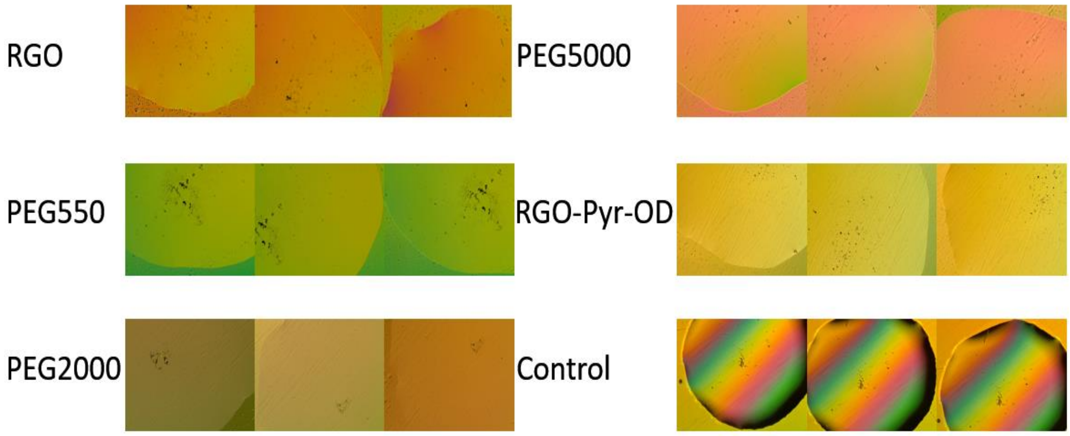

Supporting Figure 8. Polarized light microscope images of Kit 4 on the first day

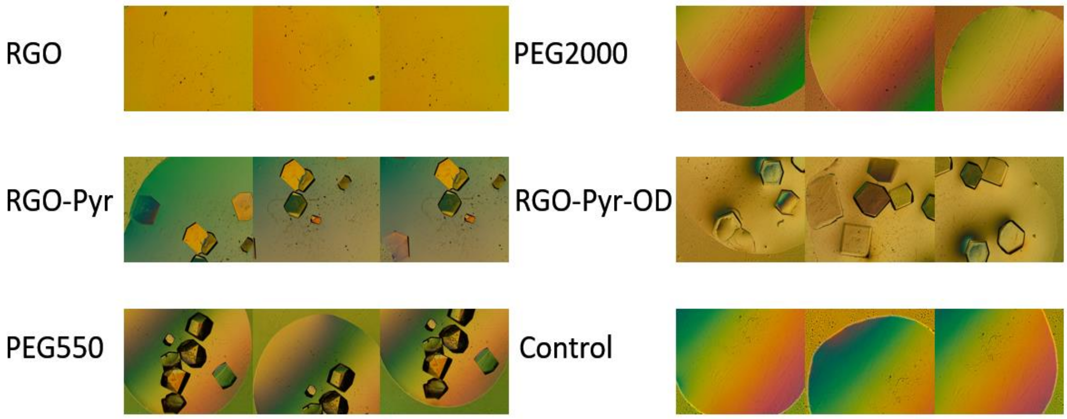

Supporting Figure 9. Polarized light microscope images of Kit 1 on the second day

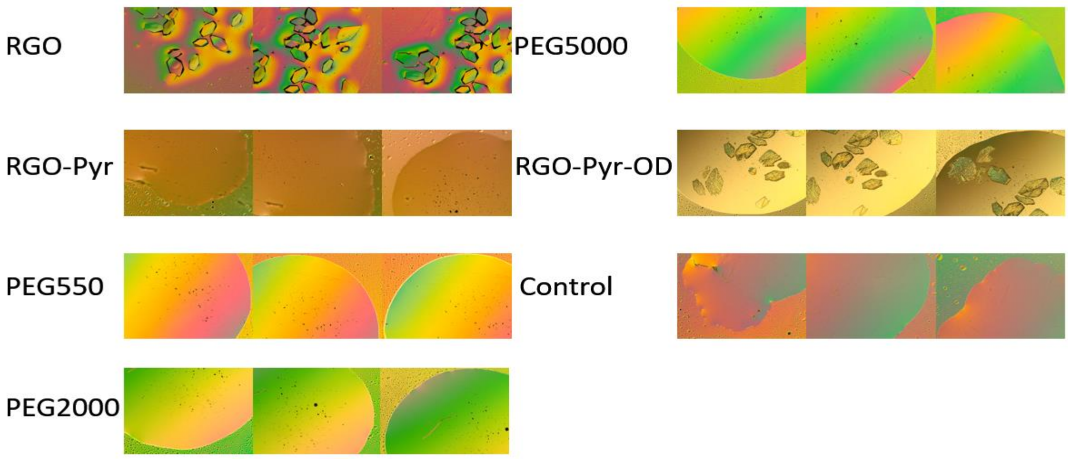

Supporting Figure 10. Polarized light microscope images of Kit 2 on the second day

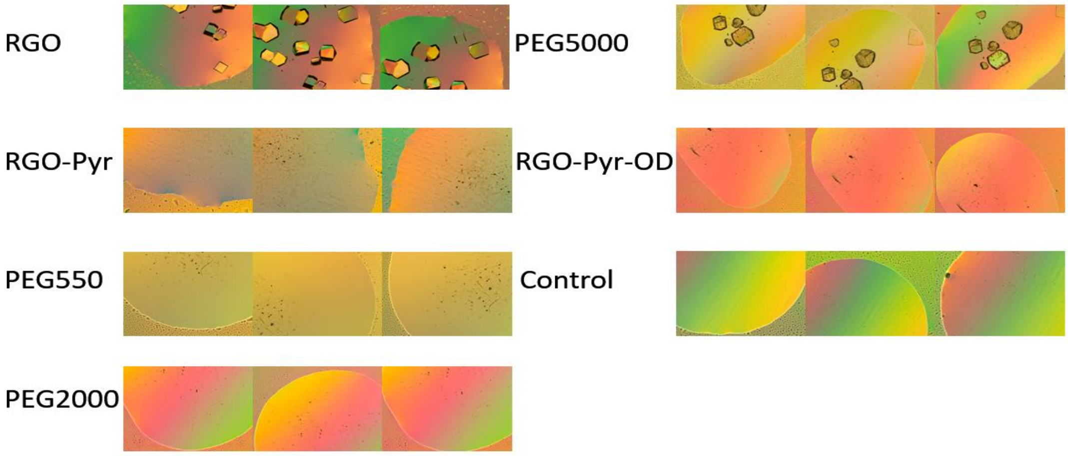

Supporting Figure 11. Polarized light microscope images of Kit 3 on the second day

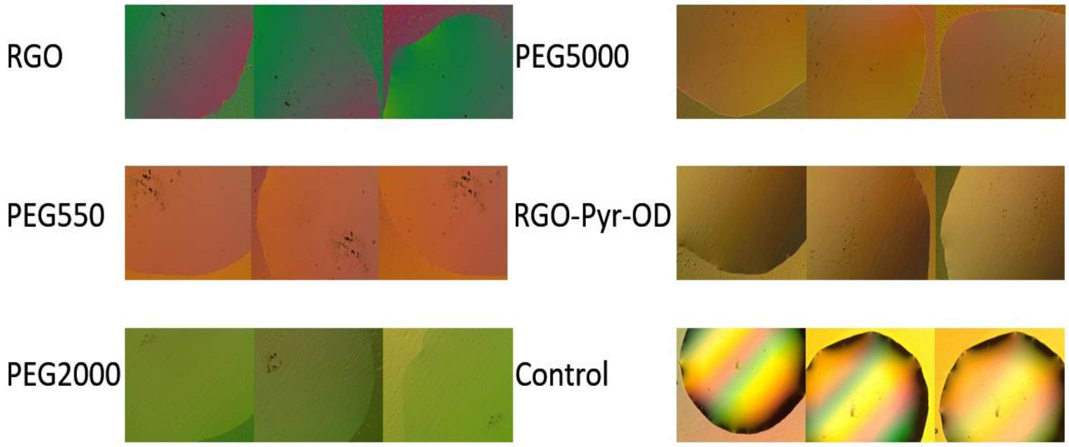

Supporting Figure 12. Polarized light microscope images of Kit 4 on the second day

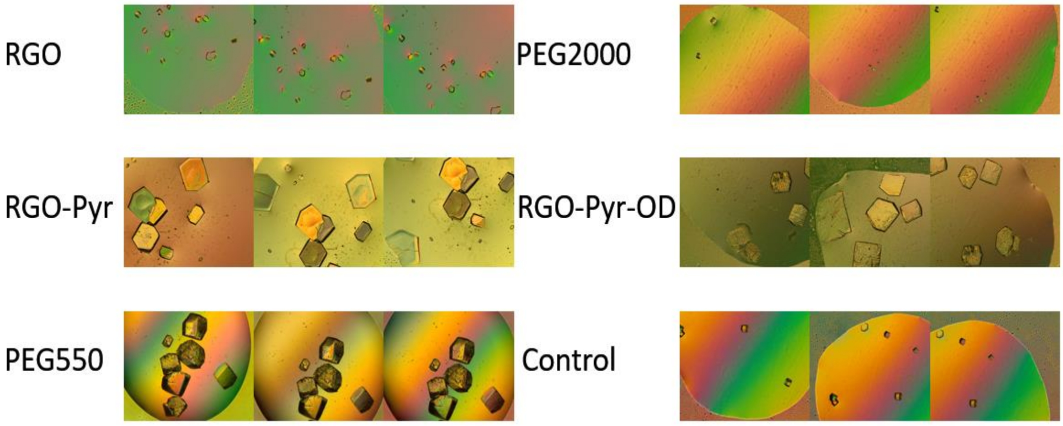

Supporting Figure 13. Polarized light microscope images of Kit 1 on the third day

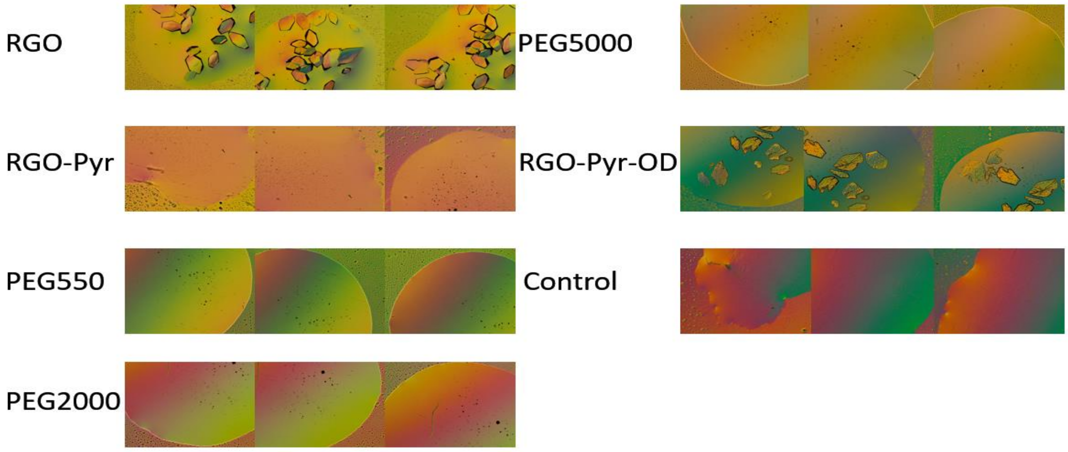

Supporting Figure 14. Polarized light microscope images of Kit 2 on the third day

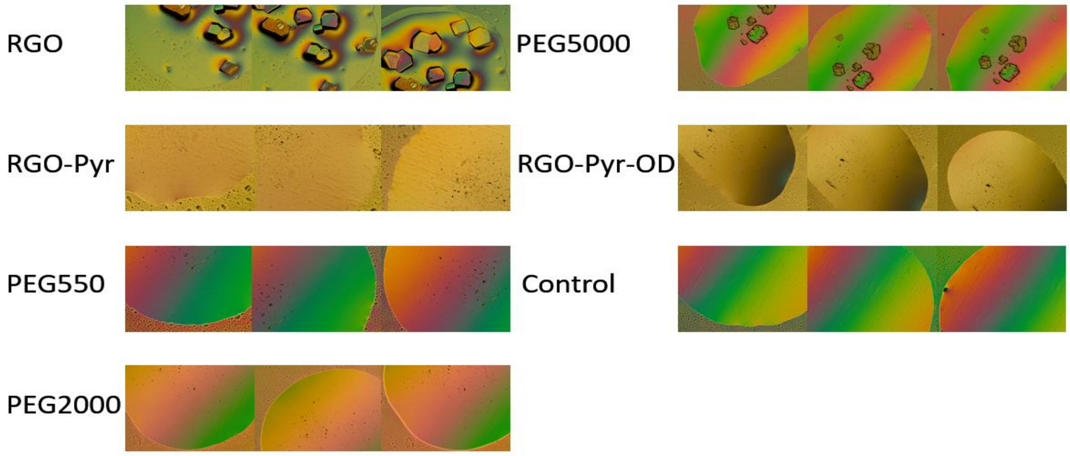

Supporting Figure 15. Polarized light microscope images of Kit 3 on the third day

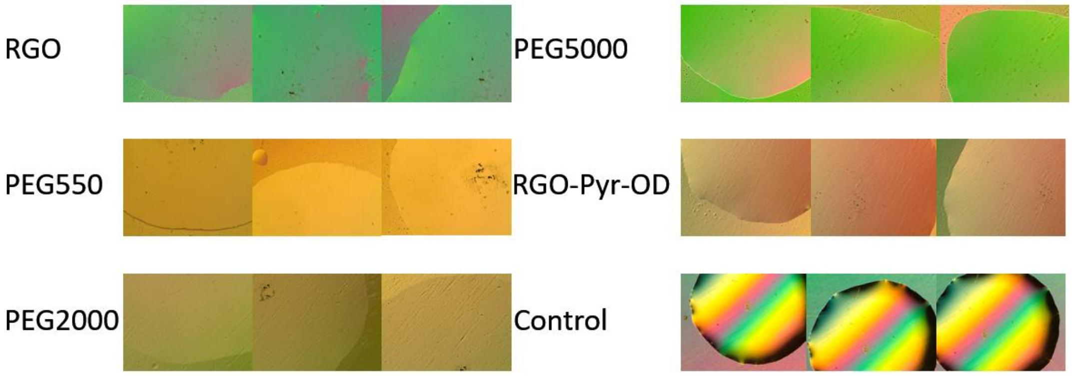

Supporting Figure 16. Polarized light microscope images of Kit 4 on the third day

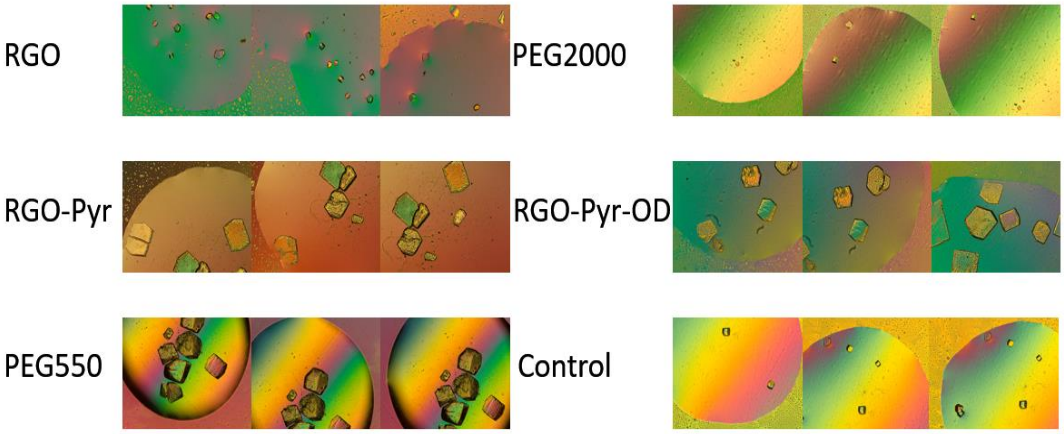

Supporting Figure 17. Polarized light microscope images of Kit 1 on the fifth day

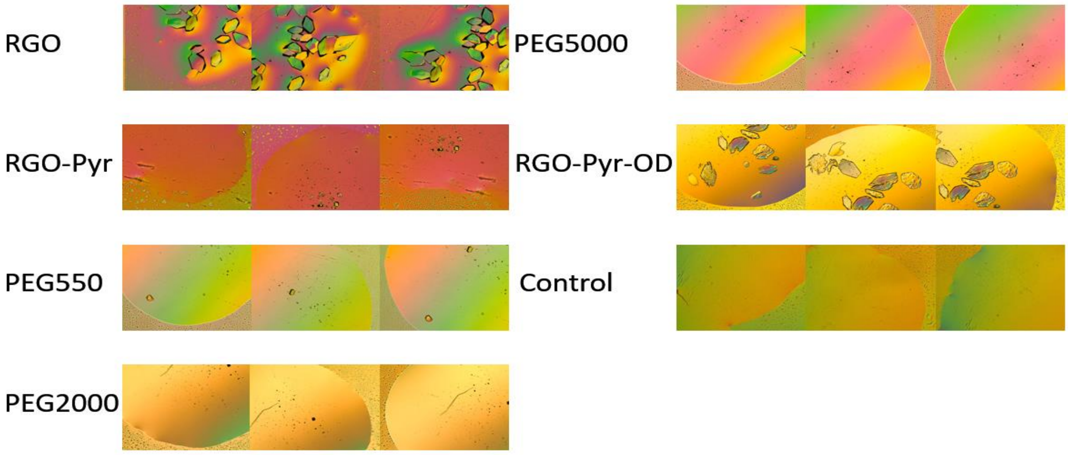

Supporting Figure 18. Polarized light microscope images of Kit 2 on the fifth day

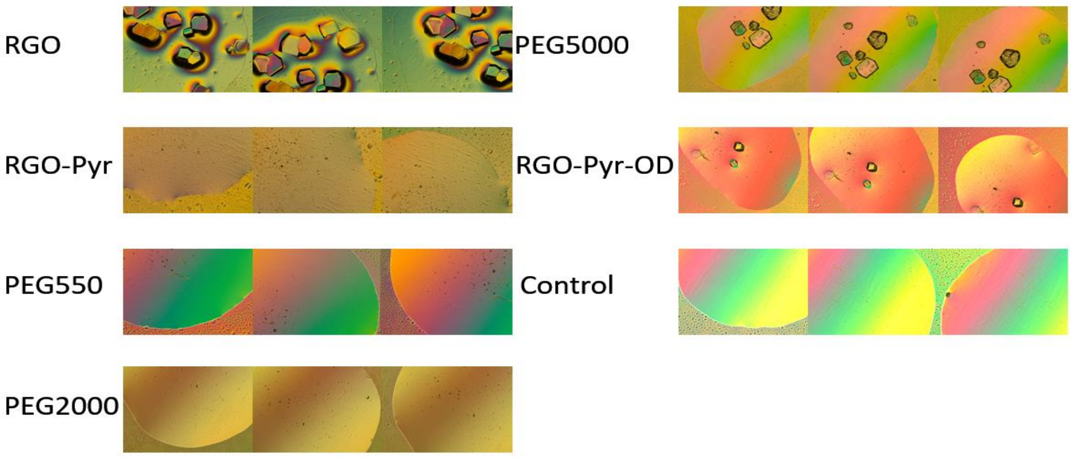

Supporting Figure 19. Polarized light microscope images of Kit 3 on the fifth day

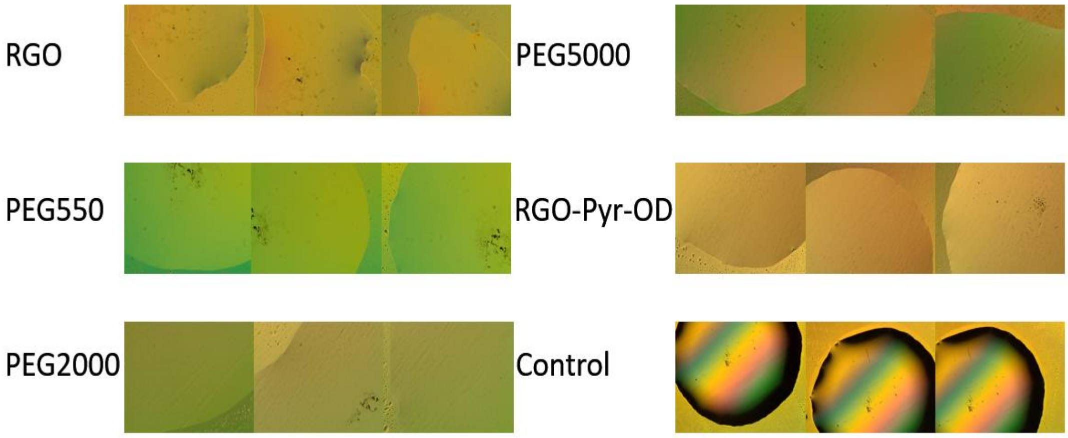

Supporting Figure 20. Polarized light microscope images of Kit 4 on the fifth day

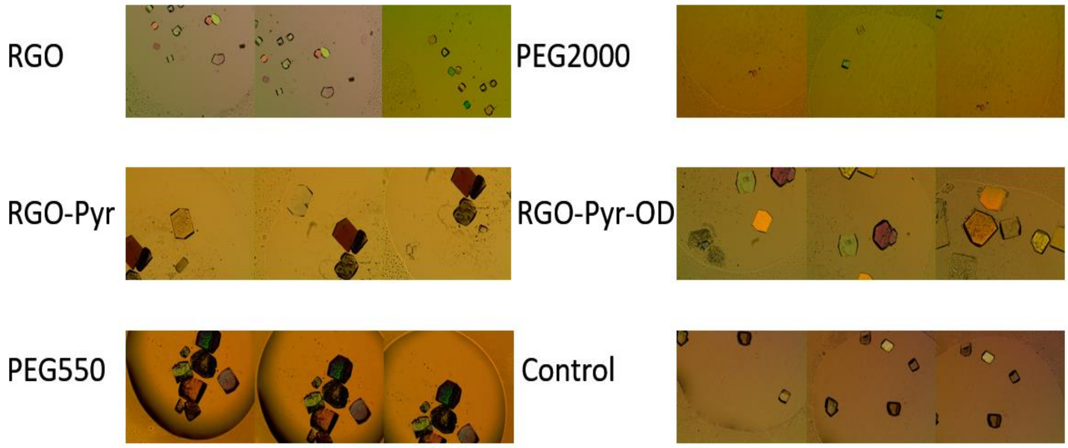

Supporting Figure 21. Polarized light microscope images of Kit 1 on the twelfth day

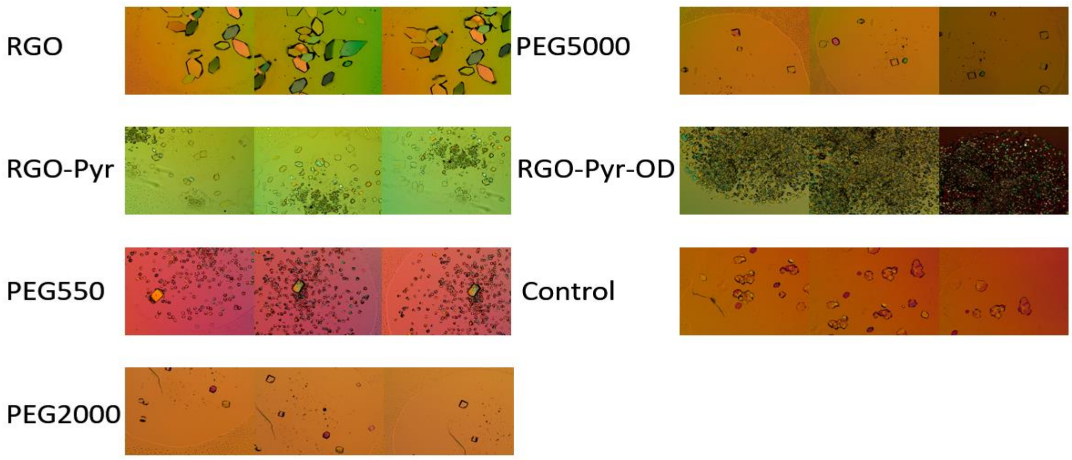

Supporting Figure 22. Polarized light microscope images of Kit 2 on the twelfth day

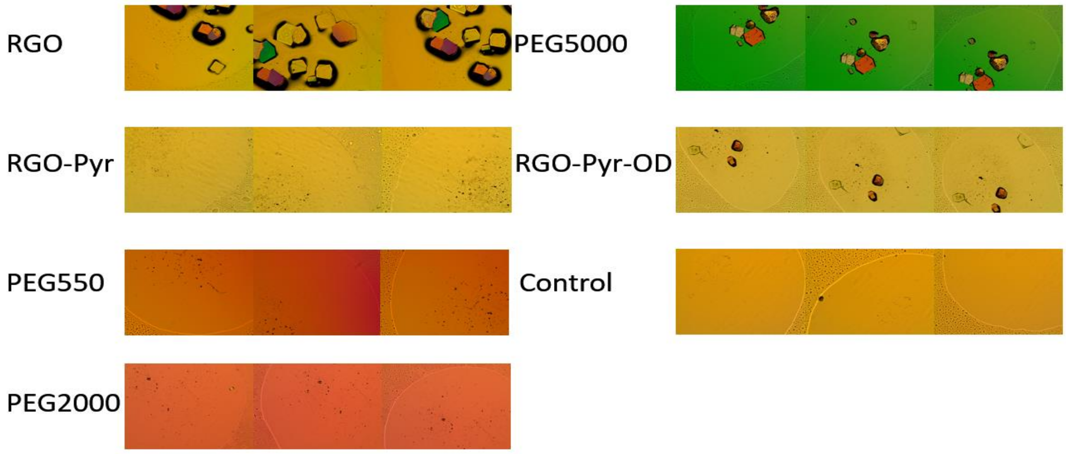

Supporting Figure 23. Polarized light microscope images of Kit 3 on the twelfth day

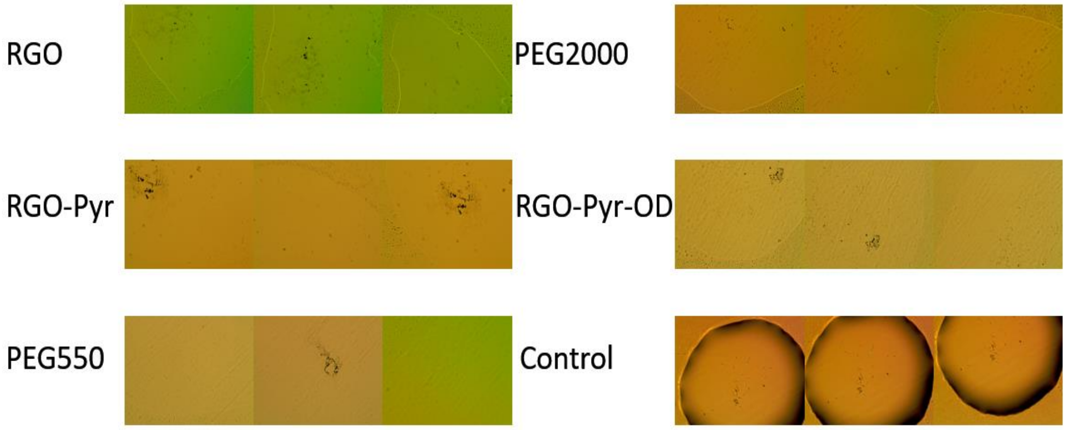

Supporting Figure 24. Polarized light microscope images of Kit 4 on the twelfth day